Real-Time EEG Response to Pulsed Transcranial Photobiomodulation in Healthy Young Adults: Effects of Stimulation Parameters and Skin Tone

Alicia Mathew[1], Hannah Van Lankveld[1,2], Xiaole Z. Zhong[1,3], Joanna X. Chen[1,2] and J. Jean Chen[1,2,3]

1 - Rotman Research Institute at Baycrest, Toronto, ON, Canada;
2 - Department of Biomedical Engineering, University of Toronto, Toronto, ON, Canada;
3 - Department of Medical Biophysics, University of Toronto, Toronto, ON, Canada

ABSTRACT

Transcranial photobiomodulation (tPBM) is a non-invasive technique that harnesses near-infrared (NIR) light to modulate brain activity. Despite growing evidence of its cognitive and electrophysiological benefits, the *in vivo* mechanisms and dose-response characteristics of tPBM remain underexplored, especially in relation to differences in skin pigmentation. Our study investigates real-time EEG responses to pulsed tPBM in 46 healthy young adults across a wide range of skin tones, quantified using individual topography angle (ITA) metrics. Participants received stimulation to the right prefrontal cortex using varied combinations of wavelength (808 vs. 1064 nm), frequency (10 Hz vs. 40 Hz), and irradiance (100, 150, and 200 mW/cm^2). EEG spectral power and sample entropy were assessed across five canonical frequency bands (delta, theta, alpha, beta, and low gamma) during and after stimulation. Our findings revealed frequency- and region-specific neuromodulation, with 1064 nm and 40 Hz parameters consistently enhancing widespread beta and gamma power, and 808 nm at 40 Hz yielding the most robust alpha power increases, contrary to the initial hypothesis that 10 Hz stimulation would elicit greater alpha enhancement. Entropy changes were more transient and stimulus-bound, while power effects, particularly in alpha and gamma bands, showed sustained post-stimulation persistence. Notably, lighter skin tones and higher irradiance were consistently associated with greater EEG modulation, highlighting the significant impact of melanin-related light attenuation on PBM efficacy. These results underscore the importance of individualized stimulation protocols and establish EEG as a powerful tool for mapping dose- and biophysical-dependent effects of pulsed tPBM in humans.

1 INTRODUCTION

Transcranial photobiomodulation (tPBM) is a non-invasive neurostimulation approach that delivers red to near-infrared (NIR) light (600-1100 nm) through the scalp to enhance cortical function by boosting mitochondrial metabolism. tPBM has been shown to engage mechanisms such as cytochrome c oxidase (CCO) activation and, more recently, endothelial nitric oxide synthase (eNOS) phosphorylation, leading to enhanced ATP production, neuroprotection, and cerebral blood flow (CBF) (Hennessy and Hamblin, 2017; Hamblin, 2018; Salehpour et al., 2018; Vargas et al., 2017; Yokomizo et al., 2022). Correspondingly, both single and repeated sessions have been associated with cognitive improvements, including enhanced attention, reaction time, working memory, and executive function across age groups (Gonzalez-Lima and Barrett, 2014; Vargas et al., 2017; Chan et al., 2019). These outcomes are typically assessed using cognitive tests, which, while widely accepted, are subjective and prone to confounding influences (Hess et al., 2020). Objective neural markers are therefore essential for understanding the mechanisms of tPBM – one such marker being brain activity measured via electroencephalography (EEG) (Shetty et al., 2023).

EEG offers a temporally precise, non-invasive window into brain function, with well-characterized cognitive associations for its canonical frequency bands (delta, theta, alpha, beta, gamma) (**Table 1**) (Berger, 1929; Nunez and Srinivasan, 2005). While EEG oscillations vary with brain state (e.g., eyes open/closed, task engagement) and individual traits (e.g. sex, age), consistent patterns emerge in aging and disease. For instance, normal aging is linked to reductions in theta and alpha power, while Alzheimer's disease (AD) often presents with elevated delta/theta and reduced alpha/beta/gamma power (R.E. Dustman, D.E. Shearer, Y. Emmerson, 1993; López-Loeza et al., 2016; Scally et al., 2018; Jabès et al., 2021; Stacey et al., 2021; Babiloni et al., 2020). These patterns make EEG a valuable tool for assessing frequency-specific neural effects of tPBM.

Table 1 Brain frequency bands and the relative clinical and cognitive significance of their power.

Band	Range	Clinical/Cognitive Significance	References
Delta	0.5 - 4 Hz	Elevated in AD and neurological disorders; may serve compensatory functions in older adults	Ai et al., 2024; Knyazev, 2012; Jeong, 2004; Jackson and Snyder, 2008; Sargent et al., 2021
Theta	4 - 8 Hz	Elevated resting-state correlates with decreased cognitive performance; decreases with aging; can support cognition in older adults	Sargent et al., 2021; Finnigan and Robertson, 2011; Vlahou et al., 2014
Alpha	8 - 13 Hz	Critical for attentional processes via inhibitory control; positively associated with cognitive performance and memory function	Palva et al., 2010; Smit et al., 2009; Klimesch et al., 1997; Mahjoory et al., 2019
Beta	13 - 30 Hz	Maintains ongoing cognitive operations; supports cognitive flexibility; optimal levels essential for efficient information processing	Buschman and Miller, 2007; Engel and Fries, 2010
Gamma	> 30 Hz	Facilitates communication between brain regions; stronger connectivity associated with enhanced cognition; 40 Hz stimulation shows promise in AD research	Liu et al., 2022; Iaccarino et al., 2016; Ballard et al., 2011; Brenowitz et al., 2017; Spera et al., 2021

While several studies have demonstrated that tPBM can modulate EEG activity, findings vary. This may be driven in part by the fact that tPBM's biological effect varies across stimulation modes, wavelengths, and frequencies. For instance, Spera et al. (2021) compared continuous-wave and 10 Hz pulsed-wave 830 nm tPBM in an eyes-open condition, finding that only continuous-wave stimulation led to widespread gamma power enhancement in frontal-central regions. Similarly, Jahan et al. (2019) reported that 1064 nm stimulation of the right prefrontal cortex was associated with significant delta power reduction and improved attentional task reaction times compared to pre-stimulation. Wang et al. (2019) reported time-resolved significant increases in alpha and beta power during tPBM in the frontal to posterior regions. In contrast, Zomorrodi et al. (2019) investigated 810 nm pulsed tPBM at 40 Hz and observed augmented alpha, beta, and gamma power and reduced delta and theta power, when directed at the default mode network (DMN). Furthermore, in another comparative exploration, Tang et al. (2023) found significant gamma power enhancements compared to baseline in pulsed tPBM conditions with the following parameter combinations: 660 nm & 40 Hz, 660 nm & 100 Hz, and 850 nm & 40 Hz, suggesting that frequency-specific effects may be contingent on the wavelength used. They also reported significant alpha power reduction after continuous-wave 850 nm tPBM compared to pre-stimulation.

While these studies highlight the potential of tPBM to modulate specific EEG bands, the interplay of key parameters, such as pulsation frequency, wavelength, irradiance, and individual factors like skin tone remains unclear. Since the efficacy of tPBM hinges on optimizing these parameters, there is a rising need for investigations into the multidimensional dependencies that shape EEG-based tPBM responses. Regarding the choice of wavelength, Monte Carlo simulations indicate that 808 nm light yields higher fractional energy deposition in cortical tissue compared to other wavelengths, with significantly greater penetration in lighter skin tones (Cassano et al., 2019; Li et al., 2017; Van Lankveld et al., 2024), implying possible wavelength-skin tone interactions. Some aspects of the dependence have been confirmed experimentally. Wang et al. (2019) found that 808 nm effectively activates CCO, while 1064 nm penetrates deeper into tissue. Yokomizo et al. (2022) demonstrated that both 808 nm and 1064 nm can enhance nitric oxide (NO) bioavailability in endothelial cells, with 1064 nm achieving deeper penetration depths due to minimal scattering and tissue absorption (Kashiwagi et al., 2014; Cao et al., 2019; Chinnathambi and Shirahata, 2019). Modeling studies also suggest that irradiance of at least 75–100 mW/cm² are required to deliver effective doses to cortical depths of 1-2 cm, with optimal physiological effects observed in the 75–250 mW/cm² range (Henderson and Morries, 2015; Wang et al., 2016; Zein et al., 2018). Moreover, a biphasic fluence dependence has been documented for PBM, with the mitochondrial response peaking at low to intermediate instead of high energy depositions (Huang et al., 2009). Critical for pulsed tPBM, the dependence on pulsation frequency also needs to be considered. It has been suggested that 10 Hz aligns with intrinsic alpha rhythms and may enhance it through entrainment, whereas 40 Hz aligns with gamma oscillations, central to higher-order cognitive processing (Iaccarino et al., 2016; Zomorrodi et al., 2019). However, this behaviour has yet to be demonstrated experimentally.

Beyond light properties, skin pigmentation can also greatly influence light propagation to deep tissues and therefore, response magnitude. Melanin is a strong absorber of NIR light (Sandell and Zhu, 2011), potentially attenuating therapeutic light delivery in high melanin level individuals, contributing to variability in treatment efficacy across populations. This effect has been demonstrated through simulations, but never experimentally.

In this study, we aim to evaluate how wavelength, irradiance, pulsation frequency, and skin pigmentation interact to influence spectral power and sample entropy in the five canonical EEG frequency bands from healthy adults undergoing right prefrontal tPBM. We hypothesize that (i) 10 Hz will preferentially enhance alpha activity while 40 Hz will augment gamma power, (ii) 1064 nm stimulation will elicit the strongest EEG responses via deeper tissue penetration, (iii) higher irradiance levels will produce stronger EEG responses, and (iv) lighter skin tones will be associated with greater EEG modulation due to more efficient dose delivery.

2 METHODS

2.1 Participants

A total of 46 healthy young adults (aged 20-32) were recruited through the Baycrest Participants Database, consisting of individuals from Baycrest and local communities, including 22 females (mean age = 23.0 ± 2.8 years) and 24 males (mean age = 26.0 ± 3.4 years). Each participant underwent four EEG scans with simultaneous tPBM stimulation. Individuals were screened to exclude any history of neurological or physiological disorders, malignant disease, or use of recreational substances that could confound EEG data. Ethical approval was obtained from the Baycrest Research Ethics Board and all participants provided written informed consent.

2.1.1 Melanin Assessment and Grouping

To account for individual differences in skin optical properties that may affect light penetration during tPBM, we measured forehead skin pigmentation using a CM-600D spectrophotometer (Konica Minolta, Tokyo, Japan). The device outputs colorimetric values in the CIE L^* b^* color space, where L^* represents luminance (0 = black, 100 = white), and b^* represents the blue-yellow axis. For each participant, six readings were taken over an 8-mm diameter area on the right forehead and averaged. These L^* and b^* values were used to compute individual topography angles (ITA), a skin pigmentation index resulting from both eumelanin and pheomelanin, defined as:

$$ITA = arctan(\frac{L^*-50}{b^*}) \times \frac{180}{\pi} \quad (1)$$

Using a reference of L = 50, the ITA is the angle formed by the L^* (luminance) and b^* (blue-yellow) axes, with higher ITAs corresponding to lighter skin tones. Both black and white calibration were performed prior to measurement to ensure accuracy.

Efforts were made to ensure a broad coverage of different skin tones across experimental protocols. Participants can be grouped into three skin-tone groups based on custom ITA thresholds (**Table 1** and **Figure 1**), consistent with previous literature (Jung et al., 2023). We also ensured an even ratio of males and females in each skin-tone group (Groups 1, 2, 3) (**Table 2**). Continuous ITA values were retained for all statistical analyses to better capture individual-level variation in skin light absorption during tPBM.

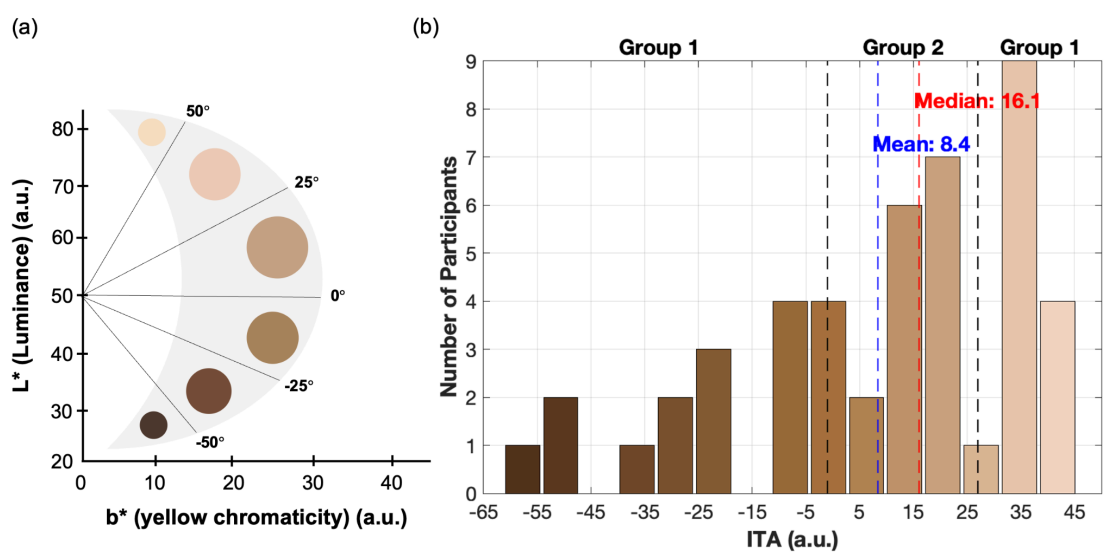

Fig 1 (a) ITA as a quantification of skin tone. (b) Participant distribution across ITAs (median ± range = 16.1 ± 106.7), with the mean and median in blue and red respectively, and group (Groups 1, 2, 3) boundaries in black.

2.2 Photobiomodulation Setup and Stimulation Parameters

Participants received NIR stimulation to the right prefrontal cortex (rPFC) using two laser systems: MDL-III-808-1W and MDL-III-1064-1W (Vielight Inc., Toronto, Canada), which delivered 808 nm and 1064 nm light, respectively. Light was transmitted via a 400 µm optical fiber to a custom headpiece secured on the participant's forehead (**Figure 2a**). This target site was selected based on prior work demonstrating cognitive improvements following rPFC stimulation (Wang et al., 2019; Jahan et al., 2019; Shahdadian et al., 2022).

The systems operated at a 50% duty cycle, meaning the laser was active for half the duration of the stimulation period. To reduce expectancy effects, stimulation parameters were remotely controlled and participants were blinded to the specific protocol and study design. Although no formal sham stimulation was incorporated, each scan included a pre-stimulation baseline phase to serve as a within-subject control. Additionally, participants were asked to report any noticeable thermal sensations during stimulation; none were reported.

Three distinct stimulation protocols (P1, P2, and, P3) were designed using combinations of two wavelengths (808 nm, 1064 nm), two pulsed frequencies (10 Hz, 40 Hz), and three irradiance levels (100, 150, 200 mW/cm²). Each participant was randomly assigned to a protocol and completed four EEG scans, each with a unique parameter configuration (**Table 2**). The number of participants per melanin group per protocol was as balanced as possible. A detailed list of treatment parameters can be found in **Table 3**.

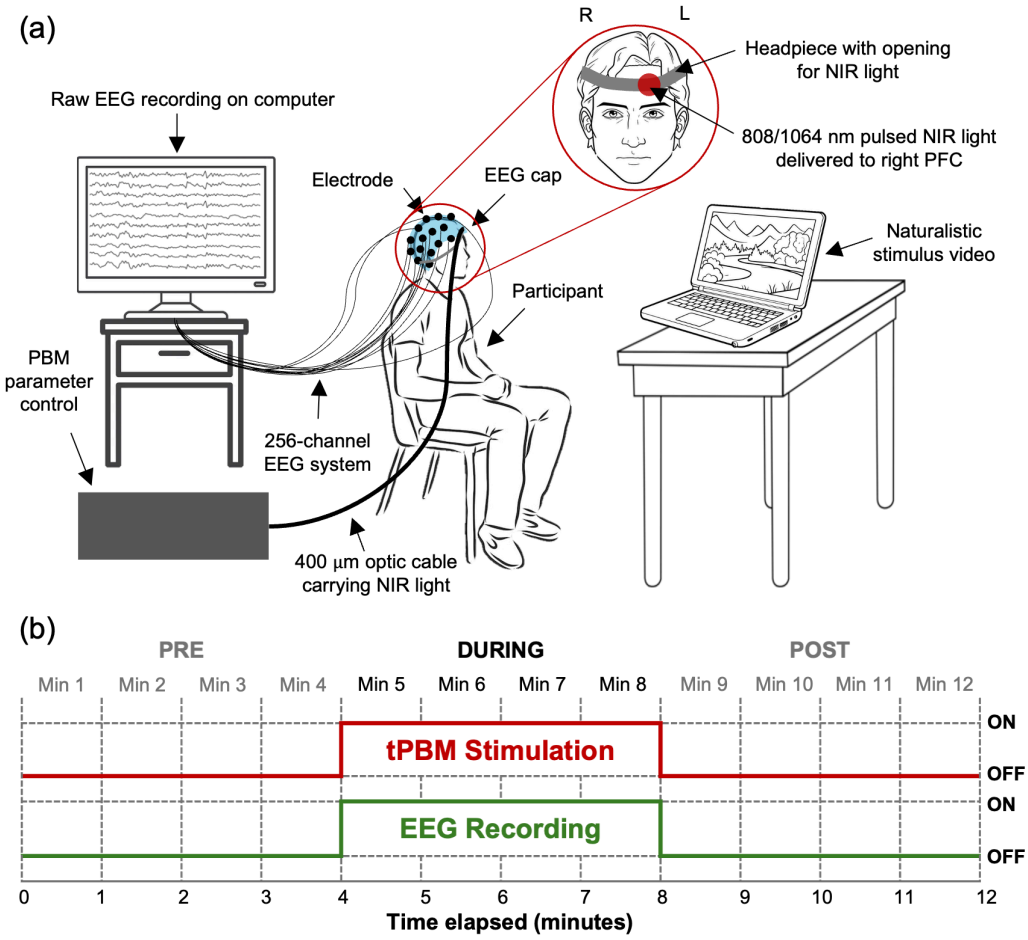

Fig 2 (a) Illustration of EEG-tPBM experimental setup. (b) Single EEG scan timeline following block design.

Table 2 Participant distribution by melanin group and protocol with specific parameter combinations.

Skin Tone Group	ITA Range	P1	P2	P3	Total	Male/Female
Group 1	27° < ITA ≤ 55°	5	5	4	14	6 M / 8 F
Group 2	-1° < ITA ≤ 27°	6	5	6	17	9 M / 8 F
Group 3	ITA ≤ -1°	5	4	6	15	9 M / 6 F
Number of Subjects		16	14	16	46	
Number of Scans		64	56	64	184	

Scan #	Protocol 1 (P1)	Protocol 2 (P2)	Protocol 3 (P3)
1	1064 nm, 100 mW/cm², 10 Hz	1064 nm, 150 mW/cm², 10 Hz	1064 nm, 150 mW/cm², 40 Hz
2	808 nm, 100 mW/cm², 10 Hz	808 nm, 150 mW/cm², 10 Hz	808 nm, 150 mW/cm², 40 Hz
3	1064 nm, 200 mW/cm², 10 Hz	1064 nm, 200 mW/cm², 40 Hz	1064 nm, 200 mW/cm², 40 Hz
4	808 nm, 200 mW/cm², 10 Hz	808 nm, 200 mW/cm², 40 Hz	808 nm, 200 mW/cm², 40 Hz
M/F	8 M / 8 F	7 M / 7 F	9 M / 7 F

Table 3 tPBM treatment parameters.

Parameter	Value
Beam spot size at stimulation site (cm^2)	1 cm^2
Wavelength (nm)	808 or 1064
Distance from scalp (cm)	~0
Pulsation frequency (Hz)	10 or 40
Irradiance at stimulation site (mW/cm^2)	100, 150, or 200
Duration of stimulation (minutes)	4
Fluence (J/cm^2)	12.014, 18.021, or 24.028
Radiant energy (J)	12.014, 18.021, or 24.028
Duty cycle	50%

2.3 Experimental Design and EEG Acquisition

Each EEG scan lasted 12 minutes, following a block design that included three 4-minute phases (**Figure 2b**): PRE (baseline), DURING (active stimulation), and POST (recovery). This format enabled the measurement of both online (during stimulation) and offline (post-stimulation) effects, consistent with tPBM literature (Zomorrodi et al., 2019; Wang et al., 2019). Participants sat in a dark, quiet room and viewed a naturalistic stimulus video, with the aim of reducing drowsiness and spontaneous mental activity, increasing signal reproducibility (Gal et al., 2022). Although researchers remained present, they were seated at a distance behind the participant to avoid distraction. A minimum 20-minute interval was maintained between active stimulation periods to prevent carry-over effects.

EEG recordings were acquired using a high-density 256-channel Geodesic Sensor Net with a Net Amp 400 amplifier (Magstim Inc., Roseville, MN, USA). Electrodes followed the 10-20 international placement system, with Cz as the reference, and impedance levels were kept below 50 kΩ, per manufacturer specifications for saline-based systems. EEG signals were digitized at 1000 Hz with an amplitude resolution of 0.024 μV.

2.4 EEG Data Analysis

The data analysis pipeline included preprocessing, spectral and sample entropy analysis, and linear mixed-effect modeling as shown in **Figure 3**.

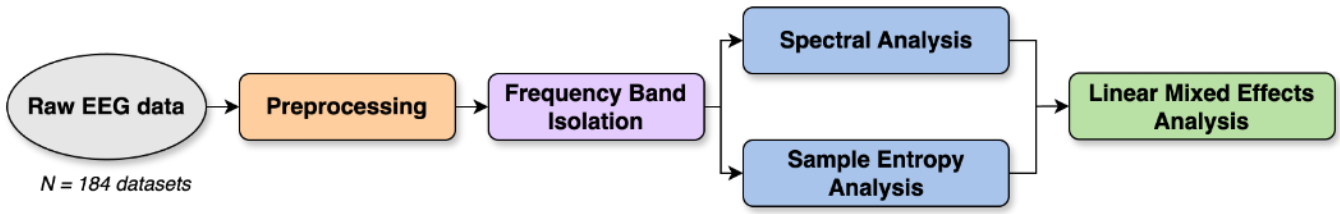

Fig 3 Illustration of key pipeline stages.

2.4.1 Preprocessing

Raw EEG data were preprocessed in MATLAB R2019b (The Mathworks Inc., Natick, MA, USA) using the EEGLAB toolbox (version 2023.1) (Delorme and Makeig, 2004). This included removing facial electrodes, downsampling to 125 Hz, and high-pass filtering at 1 Hz. Poor quality channels were identified (> 80% noisy data) and discarded using the clean_rawdata function, with additional criteria for line noise sensitivity (threshold: 4 standard deviations) and flat line segments exceeding 5 seconds.

Artifact detection utilized an extended infomax algorithm (runica function with extended option) for Independent Component Analysis (ICA). The iclabel function automatically identified and removed artifacts from muscle activity, eye movements, and line noise using a conservative threshold of 0.9.

After preprocessing, signals were further cleaned with our customized MATLAB script to enhance signal quality, which included (1) mean subtraction, (2) outlier replacement using 5th-95th percentile thresholds with nearest-neighbor interpolation, and (3) mean restoration followed by detrending to remove slow drifts.

2.4.2 Frequency Band Isolation

To perform a temporally resolved quantification of the amplitude (power) and complexity (sample entropy) of canonical EEG frequency bands in response to tPBM, we isolated narrowband signals using a custom fast Fourier Transform (FFT)-based approach. EEG data were segmented into non-overlapping 60-second epochs, each of which was multiplied by a Hann window to reduce spectral leakage.

Each windowed signal was transformed to the frequency domain using the FFT. A binary mask was then constructed to isolate the desired frequency band: delta (1-3 Hz), theta (4-8 Hz), alpha (9-12 Hz), beta (13-30 Hz), and low gamma (30-50 Hz). This mask was mirrored across negative frequencies to preserve conjugate symmetry, ensuring a real-valued inverse transform. The resulting band-limited signal was reconstructed using the inverse FFT, yielding a time-domain waveform containing only the desired frequency content. This approach aimed to generate band-specific EEG signals suitable for both power and entropy analysis while avoiding distortions from sharp filter transitions or overlapping windows.

2.4.3 Spectral Analysis

Spectral power of each frequency band within each one-minute epoch was calculated as the variance of the time-domain signal. To account for baseline differences across individuals and electrodes, all power values were normalized to the pre-stimulation (PRE) baseline period mean and expressed as percent change (**Equation 2**):

$$P(\%) = \frac{P(t) - PBaseline}{PBaseline} \times 100 \qquad (2)$$

where P(t) is the power at time t, and PBaseline is the mean power (DC power) during the baseline period.

2.4.4 Sample Entropy Analysis

Sample entropy (SampEn) was computed on the time-domain signals to assess the temporal complexity of neural dynamics in each frequency band. This metric estimates the irregularity of the time series, with lower values indicating more regular or synchronized activity, and higher values reflecting increased signal complexity (Richman and Moorman, 2000; Mizuno et al., 2010). The calculation of SampEn can be found in the supplementary materials section. Similar to power analysis, all entropy values were normalized to the pre-stimulation (PRE) baseline period mean and expressed as percent change (**Equation 4**),

$$SE(\%) = \frac{SE(t) - SEBaseline}{SEBaseline} \times 100 \qquad (4)$$

where SE(t) is the sample entropy at time t and SEBaseline is the mean sample entropy during the baseline period.

2.4.4 Statistical Analysis

To identify spatially and temporally consistent modulations in EEG power and sample entropy, a cluster-based thresholding approach was employed using the Fieldtrip toolbox (Oostenveld et al. 2011) in MATLAB. Electrode neighbourhoods were defined using the 'distance' method applied to the GSN- HydroCel-256 channel layout, with a spatial threshold of 0.05 normalized 2D units. Electrodes within this radius were considered spatial neighbours. For each electrode, a general linear model (GLM) was applied to the minute-by-minute power or entropy time series using a binary stimulus regressor (0 = OFF, 1 = ON) that reflected the block design. Electrodes with significant stimulation effects ($p < 0.05$) were then grouped into candidate clusters if they were spatial neighbours and exhibited similar response dynamics, defined as Pearson correlation $r > 0.05$ between their time courses.

To statistically validate these clusters, we implemented a permutation-based cluster test. Each cluster's time series was averaged across its electrodes before a GLM was reapplied to the mean time course. Stimulus labels were then shuffled and this analysis was repeated 500 times to generate a null distribution of t-statistics for each cluster. A cluster was deemed significant if its mean t-statistic exceeded the permutation threshold (mean + 2 standard deviations of the null distribution). This two-stage approach allowed the control of multiple comparisons.

Electrodes within significant clusters were then classified as displaying either positive or negative modulation, based on the sign of their original GLM t-statistics, and assigned to anatomical regions (prefrontal, frontal, central, parietal, temporal, occipital). These were further subdivided by hemisphere to distinguish local effects near the rPFC stimulation site from broader network-level responses. Both power and entropy analyses followed this identical pipeline, enabling direct comparisons between changes in oscillatory magnitude and signal complexity across spatial regions and stimulation parameters.

2.4.4.1 *Linear Mixed Effects Analysis*

To assess how different stimulation parameters modulated neural activity across brain regions and time windows, we conducted a two-stage linear mixed-effects analysis on the electrodes that survived the cluster-level statistical threshold described in Section 2.4.4. Electrodes from significant clusters were grouped by anatomical region (listed above) and their time series were averaged within two temporal windows: online (minutes 6-8) and offline (minutes 10-12), reflecting periods of sustained stimulation and post-stimulation recovery, respectively. Responses were then classified as enhancement or suppression based on the direction of baseline-normalized changes in their average power or sample entropy time series.

The first stage involved using stepwise linear regression (MATLAB's stepwiselm) to identify predictors with significant contributions to the response R, either baseline-normalized power or entropy. Variables (and their interactions) were added iteratively from a constant-only model, and excluded if their effect size did not meet a $p < 0.05$ False Discovery Rate (FDR)-corrected threshold. Surviving predictors were then entered into a final stage LME model where the response variable R was modeled, for example, as:

$$R \sim Effect_1 + Effect_2 + Effect_1 : Effect_2 + (1 \mid Subject)$$

Fixed-effect variables included wavelength (808 nm or 1064 nm), pulsation frequency (10 Hz or 40 Hz), and irradiance (100, 150, or 200 mW/cm²), all encoded as categorical variables, and ITA as a continuous variable. Subject ID was used as a random effect to account for inter-individual variability. Final statistical significance was evaluated again using FDR correction, with results reported for predictors with $q < 0.05$. Through this, we hoped to identify not just where and when changes occurred, but which specific parameters contributed to those effects, and whether they were modulated by anatomical factors like skin tone.

3 RESULTS

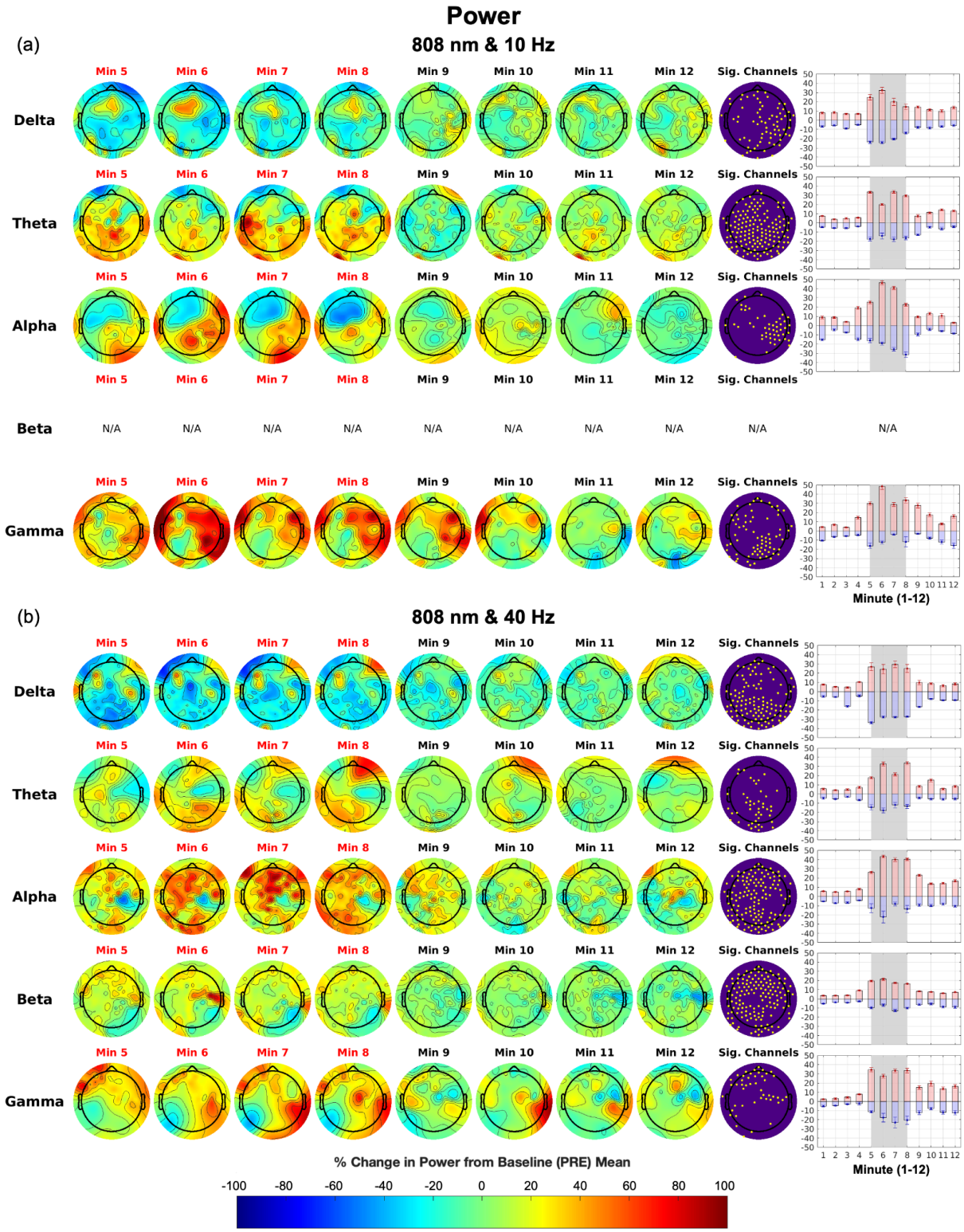

Fig 4 EEG power response to tPBM using 808 nm laser: minute-by-minute scalp topographies and time courses of baseline-normalized group-averaged EEG power in significantly responding electrodes for all frequency bands in (a) 10 Hz and (b) 40 Hz.

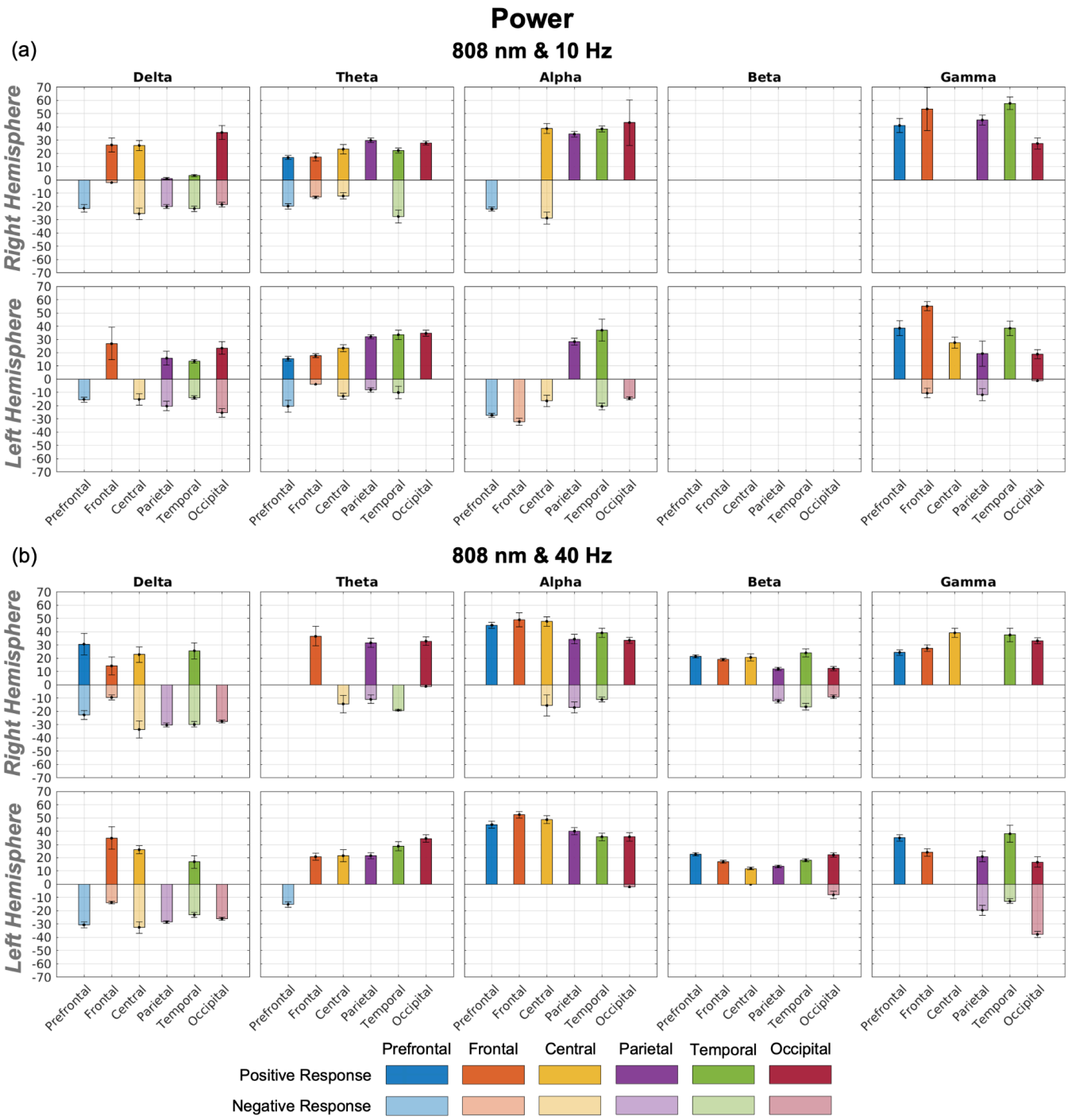

Fig 5 Bar plots representing the average significant baseline-normalized frequency band power during the last three minutes (Min 6-8) of active tPBM stimulation separated by brain region and hemisphere. This is done for both (a) 808 nm & 10 Hz and (b) 808 nm & 40 Hz wavelength-frequency groups. The error bars represent the standard error across all significant electrodes across all data sets, for each brain region.

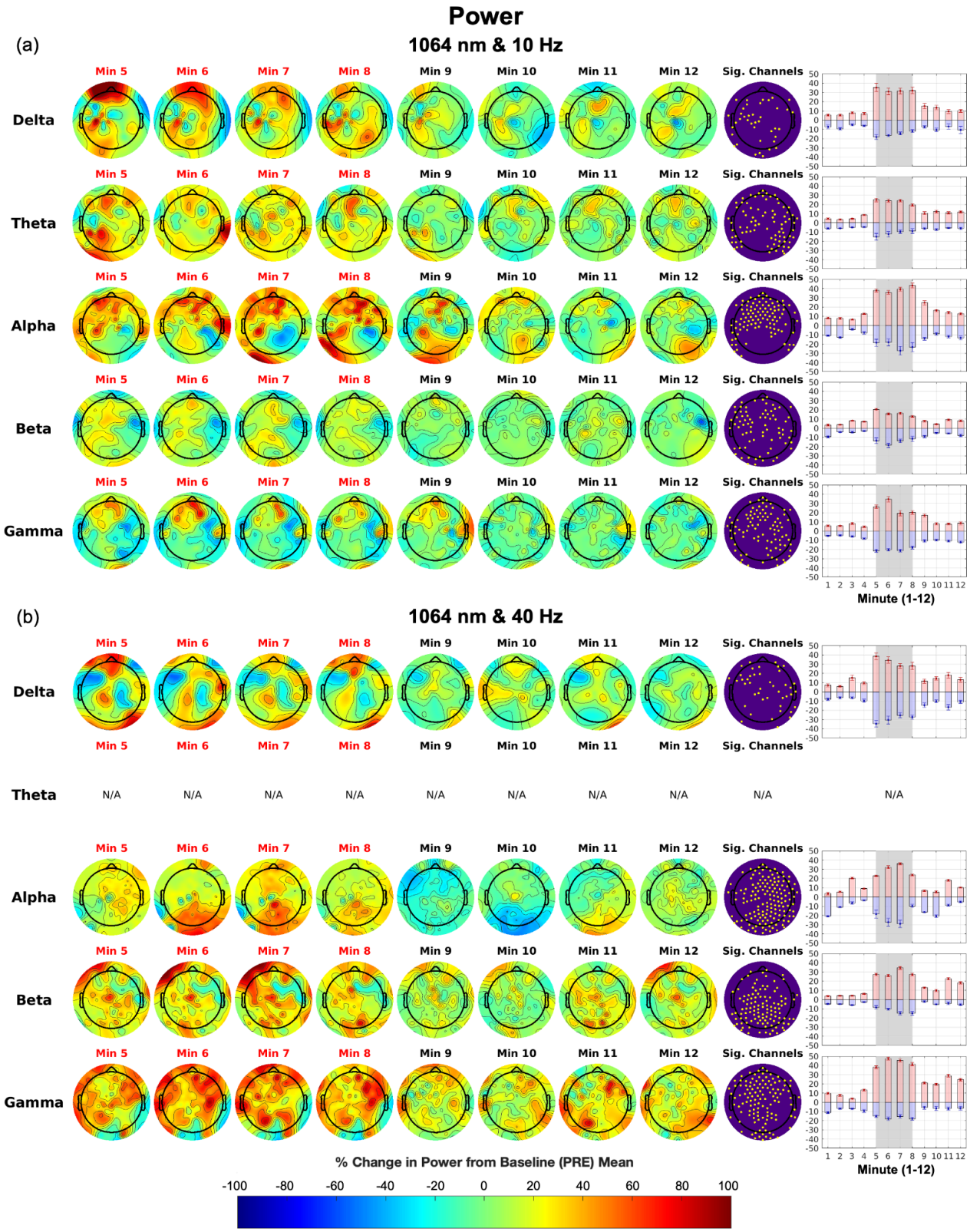

Fig 6 EEG power response to tPBM using 1064 nm laser: minute-by-minute scalp topographies and time courses of baseline-normalized group-averaged EEG power in significantly responding electrodes for all frequency bands in (a) 10 Hz and (b) 40 Hz.

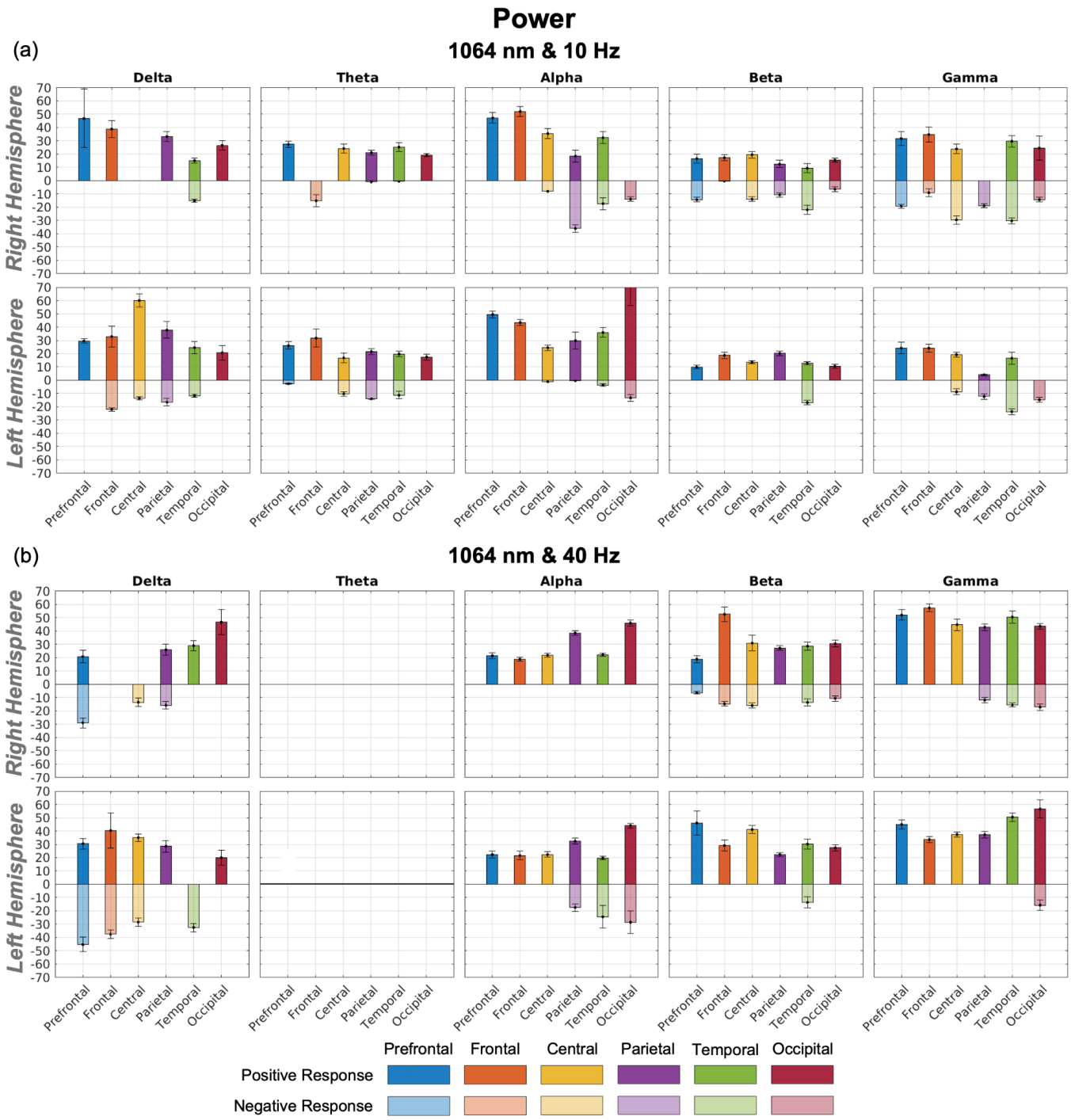

Fig 7 Bar plots representing the average significant baseline-normalized frequency band power during the last three minutes (Min 6-8) of active tPBM stimulation separated by brain region and hemisphere. This is done for both (a) 1064 nm & 10 Hz and (b) 1064 nm & 40 Hz wavelength-frequency groups. The error bars represent the standard error across all significant electrodes across all data sets, for each brain region.

3.1 Online Effect of tPBM on EEG Power

The analysis of EEG spectral power during and after tPBM stimulation to the rPFC revealed significant changes compared to the pre-tPBM baseline, with notable hemispheric and regional differences. Moreover, wavelength and frequency-specific modulations were also uncovered across all frequency bands. For conciseness, LH and RH are used to denote the left and right hemispheres, respectively. Significant activity beyond 100% change from the baseline mean were excluded. As can be seen in **Figure 4**, the onset of power changes with tPBM (online effects) was immediate, while recovery to baseline (offline effect) was more prolonged.

3.1.1 Frequency dependence at 808 nm

We will first describe the electrode topography of the responses. As shown in **Figure 4**, the contour plots of the significant responses as well as the associated electrodes are mapped for the 808 nm wavelength. The percent power responses during PBM associated with different brain regions are summarized in **Figure 5.**

At the low-frequency end, delta power showed minimal but significant enhancement during both 10 Hz and 40 Hz stimulation, with 40 Hz even exhibiting mild suppression (**Figure 5**). These patterns are quantitatively summarized in **Figure 5**, which confirms bilateral prefrontal reduction and frontal increase of delta power, with all other regions displaying both an increase and decrease in power. In comparison, at 40 Hz, **Figure 4** delta power shows consistent widespread reduction across all regions. A more detailed view in **Figure 5b** shows similar power changes in both hemispheres across multiple brain regions. Theta power appeared enhanced during tPBM across central and parietal regions (**Figure 4a**), with the LH more enhanced than the right, and 10 Hz producing more pronounced frontal power increases compared to 40 Hz (**Figure 5**).

In the intermediate range, alpha power demonstrates posterior specific enhancement during tPBM at 10 Hz and more global enhancement at 40 Hz (**Figure 4**). This is also shown by **Figure 5**, which shows consistent bilateral alpha power enhancement at 40 Hz in contrast with a more limited right-hemisphere posterior power enhancement at 10 Hz. The bar graphs also show 40 Hz stimulation as being associated with more consistent alpha-power increases than 10 Hz ($p = 4.8239e-09$, $q = 9.6479e-09$), with strong posterior enhancement for both frequencies but a more lateralized distribution in the 10 Hz condition. Beta band power showed no significant response to 10 Hz (**Figure 4a**) but displayed modest enhancement in frontal and central regions during 40 Hz stimulation (**Figure 5b**).

At the high-frequency end, gamma power exhibited the highest enhancement in the 10 Hz condition during stimulation (**Figure 4a**). This assessment is confirmed in **Figure 5**, which shows particularly high gamma power increase in right parietal and temporal regions, more so for 10 Hz than for 40 Hz. There is minimal gamma-power reduction observed.

In the 808 nm band we noted systematic differences across stimulation frequencies. With 10 Hz, significant power reduction occurred during stimulation for delta, theta, and alpha bands, whereas with 40 Hz, delta showed the most reduction, followed by alpha and gamma. Notably for the alpha band, activity shifted from being primarily within the central and anterior regions at 10 Hz to being more global at 40 Hz. Moreover, 808 nm at 40 Hz produced the greatest increase in alpha power compared to other parameter combinations, whereas 1064 nm at 40 Hz produced the greatest increase in gamma power compared to other parameter combinations.

3.1.2 Frequency dependence at 1064 nm

The 1064 nm wavelength showed distinct patterns compared to 808 nm across all bands (**Figure 6 and 7**). Starting on the low-frequency end, delta power demonstrated widespread increases with both frequencies, with 10 Hz producing stronger frontal enhancement than 40 Hz. This is confirmed by the bar graphs in **Figure 7**, which further shows that the delta increase in the prefrontal and frontal regions are stronger in the RH, with only moderate power increases shown in parietal, temporal, and occipital regions. In contrast, as seen in **Figure 7b**, at 40 Hz, the

delta-power enhancement in the right frontal and prefrontal lobes are weaker. Theta band power displayed moderately significant enhancement with 10 Hz stimulation but no significant change at 40 Hz (**Figure 6**), as confirmed in the bar graphs in **Figure 7a**.

Alpha band power showed predominant increases with both 10 and 40 Hz, more global for 10 Hz and more occipital for 40 Hz (**Figure 6**). This is confirmed in **Figure 7a**, which interestingly shows strong reduction also appeared in the right parietal region. In comparison, at 40 Hz, alpha power also showed consistent bilateral enhancement across all regions, strongest in parietal and occipital regions (**Figure 7b**). Reduction appeared only in the right parietal, temporal, and occipital regions. Notably, 1064 nm at 40 Hz produced a higher gamma-power increase than for 10 Hz ($p = 9.8222e-19$, $q = 3.9289e-18$). Beta band activity showed modest increases during 10 Hz stimulation but exhibited stronger widespread enhancement during 40 Hz stimulation, particularly in frontal to central regions. As shown in **Figure 7a**, at 40 Hz, beta activity showed consistent enhancement across all regions bilaterally, highest in the right frontal and left prefrontal regions. Lastly, gamma band power showed moderate enhancement and reduction with 10 Hz, but remarkable global enhancement at 40 Hz. As detailed in **Figure 7**, the gamma power increase at 10 Hz was second only to the alpha increase, especially in right prefrontal, frontal, and temporal regions, and more for the RH. Strong LH reductions are also seen in right central and temporal regions. The gamma increase at 40 Hz far exceeds that at 10 Hz.

To summarize, 1064 nm at 40 Hz produced the most consistent enhancement in gamma and beta bands compared to all other parameter combinations. Moreover, 808 nm at 40 Hz produced the greatest and most global increase in alpha power compared to the other parameter combinations, whereas 1064 nm at 40 Hz produced the greatest and most global increase in gamma power compared to the other parameter combinations.

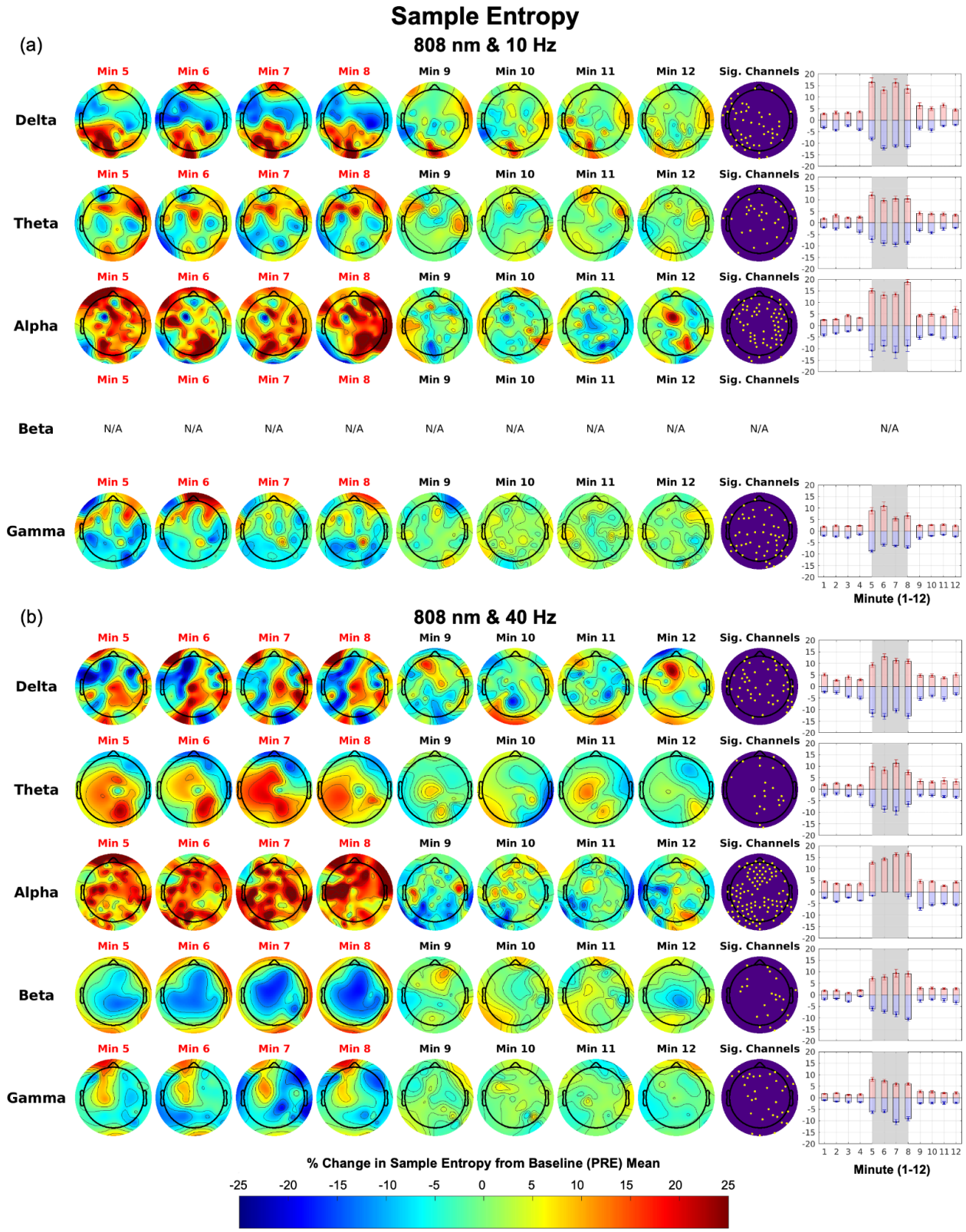

Fig 8 EEG sample entropy response to tPBM using 808 nm laser: minute-by-minute scalp topographies and time courses of baseline-normalized group-averaged EEG power in significantly responding electrodes for all frequency bands in (a) 10 Hz and (b) 40 Hz.

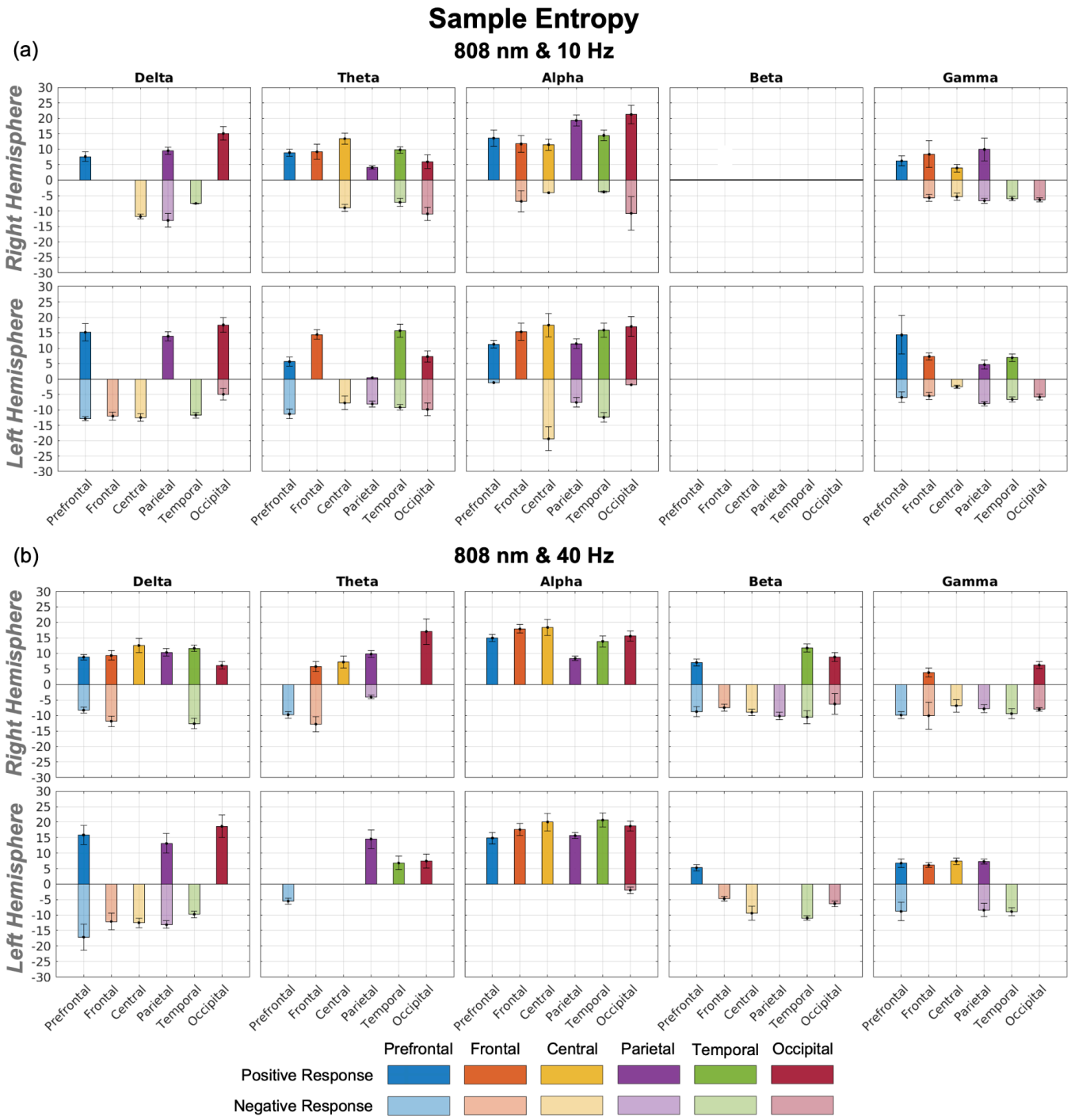

Fig 9 Bar plots representing the average significant baseline-normalized frequency band sample entropy during the last three minutes (Min 6-8) of active tPBM stimulation separated by brain region and hemisphere. This is done for both (a) 808 nm & 10 Hz and (b) 808 nm & 40 Hz wavelength-frequency groups. The error bars represent the standard error across all significant electrodes across all data sets, for each brain region.

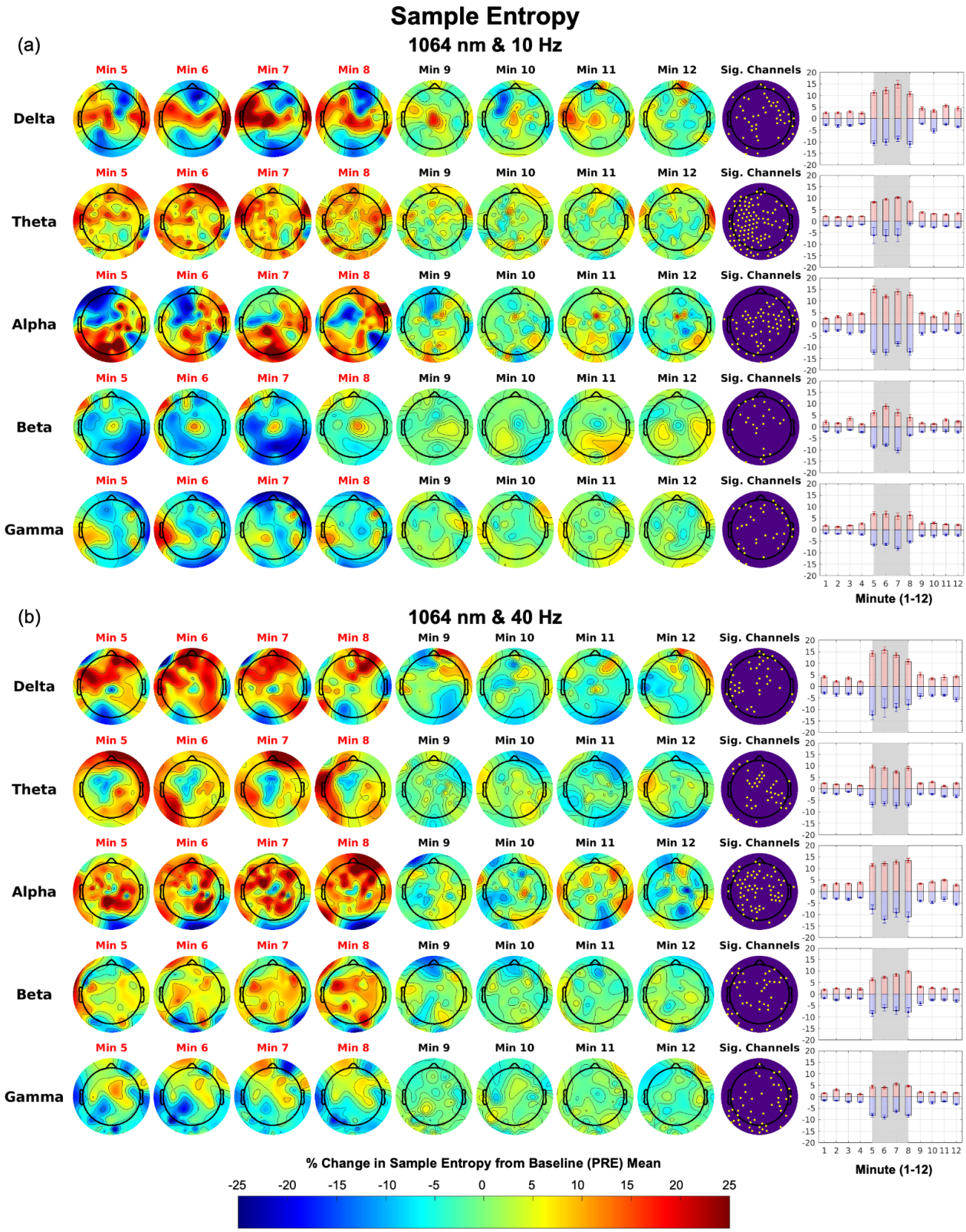

Fig 10 EEG sample entropy response to tPBM using 1064 nm laser: minute-by-minute scalp topographies and time courses of baseline-normalized group-averaged EEG power in significantly responding electrodes for all frequency bands in (a) 10 Hz and (b) 40 Hz.

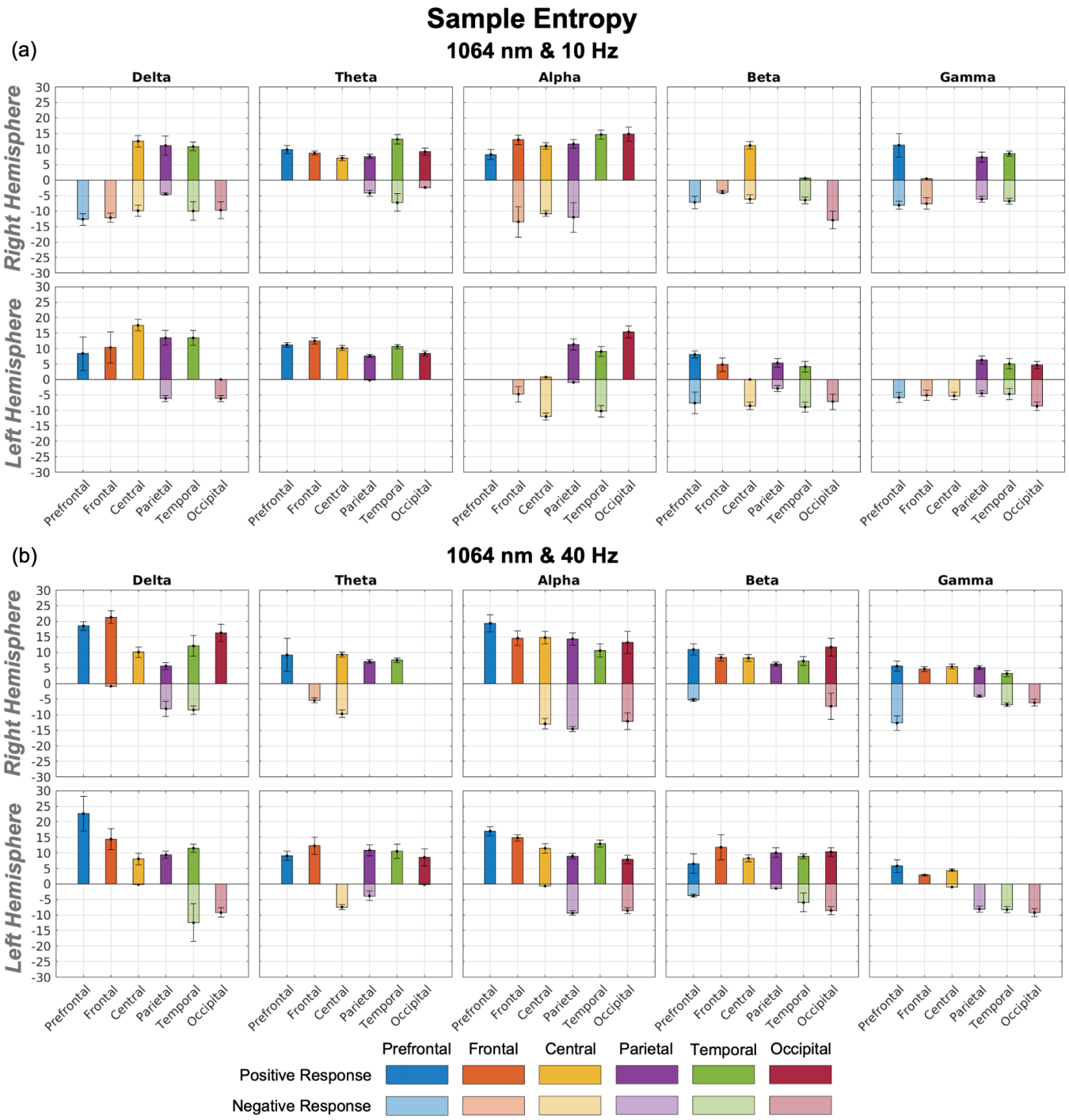

Fig 11 Bar plots representing the average significant baseline-normalized frequency band sample entropy during the last three minutes (Min 6-8) of active tPBM stimulation separated by brain region and hemisphere. This is done for both (a) 1064 nm & 10 Hz and (b) 1064 nm & 40 Hz wavelength-frequency groups. The error bars represent the standard error across all significant electrodes across all data sets, for each brain region.

3.2 Online Effect of tPBM on Sample Entropy

Similar to power, EEG sample entropy during and after tPBM stimulation displayed distinct wavelength and frequency-specific modulations across all frequency bands, with hemispheric and regional differences. As can be seen in **Figure 10**, the onset of entropy changes with tPBM (online effects) and the recovery to baseline (offline effect) were both immediate. Significant activity beyond 100% change from the baseline mean were excluded.

3.2.1 Frequency dependence at 808 nm

At 808 nm, delta entropy increased in occipital regions and decreased in central regions during 10 Hz stimulation (**Figure 8**), as quantified in **Figure 9a**. Similar patterns were observed at 40 Hz. Theta entropy remained largely unchanged at both frequencies (**Figure 8**), with slightly more right-lateralized effects at 40 Hz (**Figure 9**). Alpha entropy exhibited the strongest and most widespread increases among all bands at both 10 and 40 Hz (**Figure 8**). In the RH, increases were observed across all regions, especially in the occipital lobe, which also showed the largest entropy decreases. The LH showed a similar pattern, with strongest decreases in central and temporal areas, and smaller decreases in occipital regions compared to the RH. At 40 Hz, alpha entropy increased more markedly than at 10 Hz across all regions, with peak increases in frontal and central regions in the RH, and temporal and occipital regions in the LH (**Figure 9b**). Interestingly, entropy decreases appeared only after 40 Hz stimulation ended, unlike at 10 Hz. Beta entropy remained stable at 10 Hz but showed a global decrease at 40 Hz (**Figures 8** and **9b**). Gamma entropy exhibited minimal changes are both frequencies, with mild RH decreases during 10 Hz.

3.2.2 Frequency dependence at 1064 nm

At 1064 nm (**Figure 10**) , entropy patterns differed notably from 808 nm across all frequency bands. Delta and theta entropy increases strongly in central central, parietal, and temporal regions, with greater effects at 10 Hz than at 40 Hz (**Figure 11a**). Alpha entropy showed prominent increases in occipital regions at 10 Hz and in frontal regions at 40 Hz (particularly in the RH). However, it also showed strong frontal decreases at 10 Hz and occipital decreases at 40 Hz. Beta entropy showed limited change at either frequency. Gamma entropy showed minimal response at 10 Hz (**Figures 10a** and **11a**), but exhibited more pronounced increases during 40 Hz stimulation (**Figures 10b** and **11b**).

3.3 Offline Effect of tPBM

Post-stimulation effects (minutes 9-12) show band-specific patterns returning toward baseline, with delta power making the most rapid return for all parameter combinations. Theta power showed modest elevation in central regions after 808 nm stimulation but normalized more rapidly with 1064 nm, though the reason for this remains unclear. Alpha activity demonstrated the most persistent post-stimulation effects. Beta power, when modulated, showed mild persistence, with stronger after-effects following 1064 nm & 40 Hz stimulation compared to other combinations. Gamma activity displayed both wavelength and frequency-dependent post-stimulation effects, with 1064 nm producing the strongest power increase compared to 808 nm, and 40 Hz stimulation producing more sustained elevation compared to 10 Hz across both wavelengths. With sample entropy, tPBM effects were more acute and stimulus-dependent across the tested parameter combinations, reverting to near-baseline levels after the end of stimulation.

3.4 Multi-dimensional Dependence of tPBM Response

The two-stage LME model allowed us to concurrently observe the contributions of stimulation parameters and individual skin tone variability to the EEG response outcomes across frequency bands and brain regions. To portray the effect of categorical (wavelength, pulsation frequency, irradiance) and continuous variables (ITA) on equal footing, we converted the effect sizes (estimates) produced from the LME for the continuous variable into a "difference" size. That is, the continuous-effect estimates were scaled by the range of the variables (e.g. the range of ITA values included in the samples).

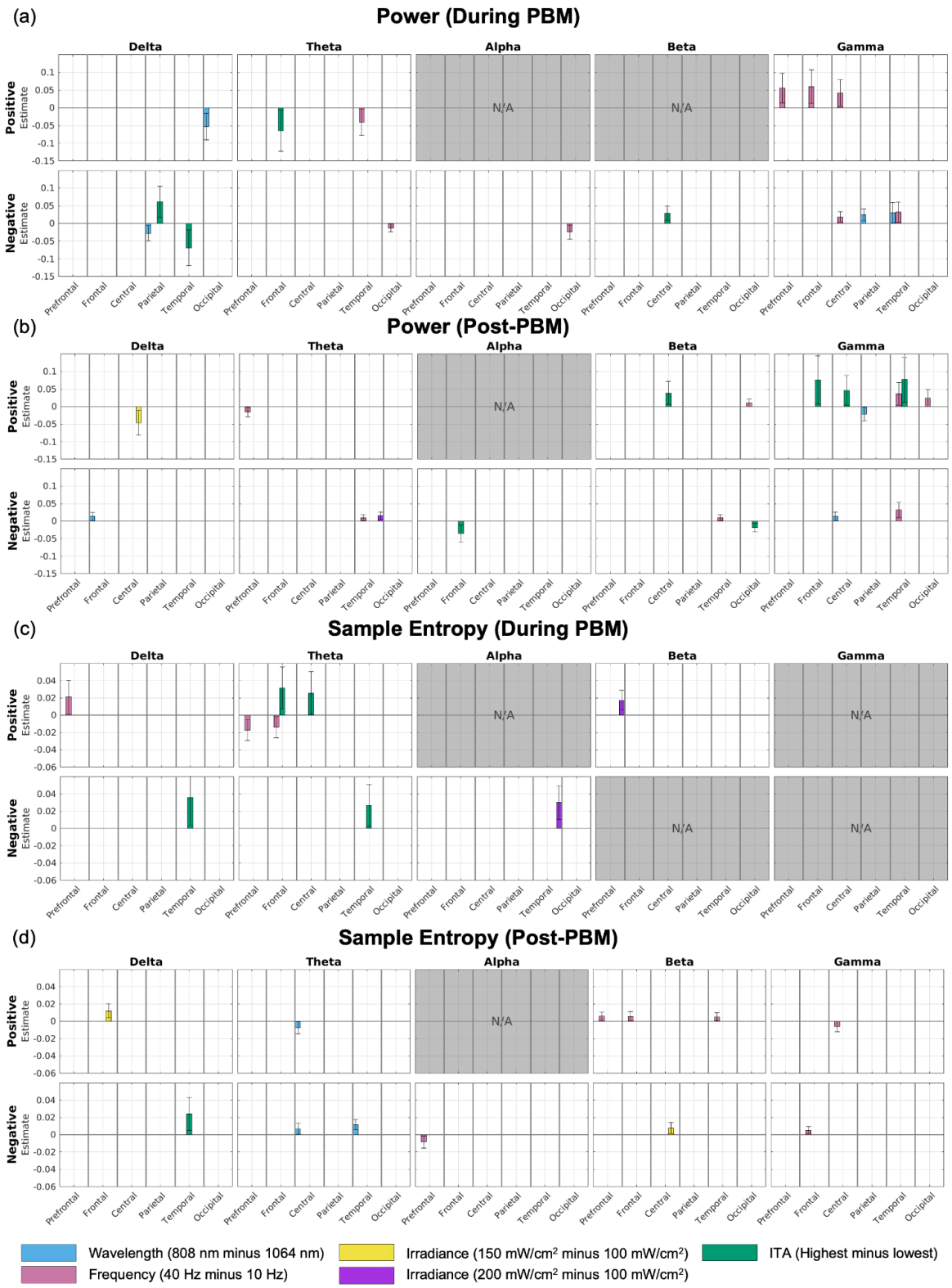

Fig 12 LME-derived estimates of significant stimulation parameters, separated by frequency band, response direction, and brain region. *Top panel*: power-based estimates (a) during and (b) post-tPBM stimulation. *Bottom panel*: sample entropy-based estimates (c) during and (d) post-tPBM stimulation. Error bars represent the 95% confidence interval.

3.4.1 Power

3.4.1.1 *Online effect (during PBM)*

The parameter and skin tone dependence of the EEG power response is summarized for each variable below. No significant interaction effects were found amongst these variables.

- **Wavelength**: Compared to 1064 nm, 808 nm was associated with weaker delta power enhancement (in the occipital region) and slightly stronger power reduction (in the parietal region). 1064 Hz was associated with stronger gamma power reduction than 808 nm in the parietal and temporal regions.
- **Frequency**: Compared to 10 Hz, 40 Hz produced weaker delta power enhancement (in the temporal region) and a stronger delta power reduction (in the occipital region). In the alpha band, 40 Hz also showed stronger reduction in the occipital region. Gamma power, however, was more strongly enhanced by 40 Hz than 10 Hz across multiple brain regions.
- **Irradiance**: No significant effects were observed for online power changes.
- **Skin tone**: Lighter skin tones (higher ITA values) were associated with more subdued delta power reduction and weaker theta power enhancement. No significant effect on other rhythms were detected.

During stimulation, gamma power showed the strongest enhancement at 40 Hz in prefrontal and frontal regions (using either wavelength) and reduction using 1064 nm and 10 Hz in the central, parietal, and temporal regions.

3.4.1.2 *Offline effect (post-PBM)*

- **Wavelength**: Compared to 1064 nm, 808 nm showed weaker reduction in frontal delta and central gamma power. Parietal gamma power also showed weaker enhancement with 808 nm than at 1064 nm.
- **Frequency**: Compared to 10 Hz, for theta power, 40 Hz showed weaker prefrontal enhancement and weaker temporal reduction. In the beta band, 40 Hz showed stronger enhancement in the occipital region and weaker reduction in the temporal region. Gamma power showed stronger temporal and occipital enhancement and weaker temporal reduction with 40 Hz.
- **Irradiance**: Compared to 100 mW/cm^2, 150 mW/cm^2 was associated with significantly lower central delta-power increase, while 200 mW/cm^2 correlated with weaker temporal theta-power reduction.
- **Skin tone**: Lighter skin tones (higher ITAs) were associated with stronger reductions in frontal alpha power and beta occipital power, as well as strong enhancements in beta power. In the gamma band, lighter skin tones are also associated with stronger enhancement in the frontal, central, and temporal regions.

Post-stimulation, the strongest enhancement occurred in gamma power at 40 Hz in lighter-skinned individuals.

3.4.2 Sample Entropy

3.4.2.1 *Online effect (during PBM)*

- **Wavelength**: No significant effects were observed for online power changes.
- **Frequency**: Compared to 10 Hz, for sample entropy, 40 Hz shows a stronger effect in prefrontal delta enhancement but a weaker effect in prefrontal and frontal theta enhancement.
- **Irradiance**: Compared to 100 mW/cm^2, 200 mW/cm^2 was associated with weaker alpha-entropy reduction in the temporal region and stronger enhancement in beta band sample entropy in the prefrontal region.
- **Skin tone**: As skin tone becomes lighter (higher ITA), we observed weaker reduction in delta band sample entropy in the temporal region. For theta band sample entropy, there was stronger enhancement in the frontal and central regions and weaker reduction in the temporal region as skin tone lightens.

During tPBM, theta entropy showed the strongest increases in lighter-skinned individuals at 10 Hz stimulation. As there was negligible offline effect on EEG entropy, multivariate dependence was not assessed.

4 DISCUSSION

This study aimed to characterize the effects of tPBM on EEG power and signal complexity, highlighting the influence of wavelength, pulsation frequency, irradiance, and skin pigmentation on the EEG power and entropy response. Interestingly, contrary to past work, we found both enhancements and reductions in the EEG metrics. Consistent with our hypotheses, we observed that 40 Hz produced more widespread increases in beta and gamma EEG power than 10 Hz tPBM, but in contrast to our hypothesis, 10 Hz tPBM did not produce stronger increases in alpha EEG power than 40 Hz. Moreover, higher irradiance levels and lighter skin tones were each linked to greater EEG responses, supporting our hypothesis that both energy delivery and skin pigmentation shape neuromodulatory outcomes. Overall, the strongest modulators of the EEG response to pulsed tPBM are skin tone and pulsation frequency. Furthermore, EEG entropy changes were more transient while spectral power exhibited more persistent post-stimulation (off-line) effects in certain frequency bands, highlighting differential temporal dynamics across EEG metrics.

4.1 tPBM and EEG Power

As introduced earlier, EEG power in different frequency bands provides insights into brain activity and various conditions. Increased theta power has been observed in early-stage depression, possibly reflecting decreased cortical activation (Grin-Yatsenko et al., 2009). Developmental changes in EEG band power have been observed in children and adolescents, with most bands decreasing in absolute power and fast bands increasing in relative power with age (Gasser et al., 1988). Moreover, reduced alpha, beta and gamma power in conjunction with increased delta and theta power have been associated with Alzheimer's disease and diabetes (Benwell et al., 2019; Hall et al., 2024).

Continuous tPBM has been shown to significantly modulate EEG rhythms. Studies have reported increases in alpha and beta band power across broad scalp regions following 1064-nm tPBM (Pruitt et al., 2024; Wang et al., 2019). Continuous tPBM also boosted gamma and beta spectral powers among healthy adults, with the largest effects observed in posterior regions (Spera et al., 2021). Pulsed tPBM at 40 Hz increased power in higher frequency bands (alpha, beta, gamma) while reducing power in lower frequency bands (delta, theta) (Zomorrodi et al., 2019). Both continuous and pulsed tPBM protocols have demonstrated effects on interhemispheric coherence and frequency entrainment (Scott et al., 2024). An interesting and persistent observation across these studies is that the EEG rhythm changes were not focal to the site of stimulation, but rather more global and extending to sites remote from the stimulation site.

Prior to this study, the combined effects of wavelength and pulsation frequency on EEG rhythms in pulsed tPBM had not been thoroughly assessed. Our spectral analysis results revealed distinct wavelength and frequency-dependent effects during right PFC stimulation. The 808 nm wavelength at 40 Hz produces the most pronounced alpha power increases across all brain regions, while 1064 nm at 10 Hz showed the strongest alpha power enhancement, particularly in prefrontal, frontal, and occipital regions. This global nature of the response is consistent with findings from previous studies using both continuous and pulsed tPBM and with different EEG system specifications (Pruitt et al., 2020, 2024; Wang et al., 2019; Zomorrodi et al., 2019). Notably, 1064 nm at 40 Hz generated the most consistent enhancement in gamma and beta bands compared to all parameter combinations, with bilateral increases across all regions. Delta power exhibited wavelength-specific responses, with 808 nm causing bilateral reductions at 40 Hz, while 1064 nm produced strong increases in prefrontal and frontal regions at 10 Hz. Post-stimulation effects were frequency-band specific, with alpha activity demonstrating the most persistent changes and delta returning most rapidly to baseline across all parameter combinations. Gamma activity displayed both wavelength and frequency-dependent post-stimulation persistence, with 1064 nm and 40 Hz producing more sustained elevation compared to other combinations.

The widespread power changes observed suggest that tPBM's effects are not merely localized but involve broader neural networks, consistent with prior studies (Hamblin, 2016; Zomorrodi et al., 2019; Jahan et al., 2019; Fekri et

al., 2019; Dmochowski et al., 2020). This global modulation may be attributed to several mechanisms. In a recent graph-theoretical EEG analysis, Ghaderi et al. (2021) demonstrated that 2.5 minutes of active 850 nm tPBM to the right medial frontal pole altered both the topological and dynamical properties of resting-state brain networks. Specifically, they reported reduced local processing and lateralization, accompanied by increased centrality in midline regions. The synthesis of network topography changes in response to tPBM will be part of our future work.

4.2 tPBM and EEG Sample Entropy

As a more novel metric that complements power, neural sample entropy is a measure of signal complexity that provides insights into brain function across various states and conditions (McDonough and Nashiro, 2014; Wang et al., 2020; Zheng et al., 2020). The general literature relates brain diseases to reduced sample EEG entropy (Cacciotti et al., 2024; Zúñiga et al., 2024) with AD patients exhibiting significantly lower sample entropy compared to healthy controls (Ando et al., 2021). However, entropy measures also track functional recovery after brain injury, with increasing sample entropy correlating with improved motor function (Cheng et al., 2019). Jia et al. (2017) also reported a negative association between sample entropy and age in normal aging, further proposing that the underlying mechanism could be a weakening of learning and memory-related networks.

This is the first study to examine the effect of tPBM on EEG band sample entropy. Our results demonstrated that tPBM induces wavelength and frequency-specific modulations in sample entropy across all frequency bands, with distinct hemispheric and regional patterns. Alpha entropy showed stronger increases with 808 nm than 1064 nm irradiation, with 40 Hz producing very strong increases across all brain regions compared to 10 Hz. In contrast, beta band entropy showed minimal changes at 10 Hz but exhibited cross-regional decreases in both hemispheres at 40 Hz. For 1064 nm stimulation, delta entropy displayed strong increases in the right central, parietal, and temporal regions at 10 Hz, with 40 Hz producing even stronger increases across all regions, particularly in prefrontal and frontal areas. Such increases could be associated with more intricate connectivity patterns between brain regions and more widespread information propagation throughout the brain (Ghaderi et al., 2021). Alpha entropy also showed distinctive patterns with strong decreases in right prefrontal and frontal regions at 10 Hz, but very strong cross-regional increases at 40 Hz, especially in the left prefrontal region. Unlike spectral power, most stimulation-induced changes in sample entropy quickly reverted to near-baseline levels post-stimulation, suggesting that tPBM's effects on neural complexity were primarily acute and stimulus-dependent rather than inducing sustained alterations in brain dynamics across the tested parameter combinations.

4.3 Pulsed PBM vs. Continuous PBM

Research suggests that pulsed PBM may offer advantages over continuous wave PBM in certain applications. Pulsed 405-nm light showed improved energy efficiency and similar antimicrobial efficacy compared to CW light for Staphylococcus aureus inactivation (Gillespie et al., 2017). For photodynamic therapy, high-intensity pulsed light demonstrated higher penetration in tissue-simulating dosimeters compared to continuous light due to transient decreases in photosensitizer absorption (Pogue et al., 1997). Moreover, pulsed tPBM generally deposits less energy, helping to minimize thermal effects (Hashmi et al., 2010). However, there is limited evidence regarding the feasibility of pulsed PBM in human neuromodulation.

In this work, we found robust and consistent EEG power and entropy changes due directly to pulsed tPBM. The findings are generally consistent with findings based on continuous PBM, with the exception that pulsed tPBM responses are also modulated by pulsation frequency. The implications of these frequencies will be discussed in more depth as follows.

4.3.1 The Influence of Pulsation Frequency

Brain stimulation at 10 Hz, an intrinsic alpha rhythm of the resting brain, has been linked to diverse effects on neural oscillations and cognition. Serving as a fulcrum between lower frequencies during sleep and higher frequencies during active cognition (Garcia-Rill et al., 2016), 10 Hz transcranial alternating current stimulation (tACS) has been shown to enhance parieto-occipital alpha activity and synchronizes cortical oscillators, modulating visual perception in a phase-dependent manner (Helfrich et al., 2014). However, it may also reduce low gamma corticomuscular coherence, pointing to cross-frequency interactions (Shahdadian et al., 2022; Wach et al., 2013). In attention tasks, 10 Hz boosts exogenous cueing, whereas 40 Hz enhances endogenous attention disengagement, suggesting distinct functional roles for alpha and gamma rhythms (Chen et al., 2022; Hopfinger, 2017).

The interest in 40 Hz stimulation is rapidly growing in light of its therapeutic promise. Notably, recent studies have explored the potential of 40 Hz sensory stimulation, particularly audiovisual, in improving brain function and treating neurological disorders such as Alzheimer's disease (Park and Tsai, 2025). This stimulation has been shown to induce gamma entrainment in the brain, with promising effects observed in Alzheimer's disease patients, including reduced ventricular dilation, stabilized hippocampal size, and improved cognitive function (Chan et al., 2022). Research has also demonstrated the feasibility of applying 40 Hz visual stimulation during sleep, effectively evoking neuronal gamma activity without degrading sleep quality (Hainke et al., 2024). Furthermore, 40 Hz light flicker has been found to alter brain electroencephalography microstates and complexity, which are implicated in various brain diseases (Zhang et al., 2021). While the exact mechanisms remain unclear, 40 Hz audiovisual stimulation has shown potential in rehabilitating brain dysfunctions related to cognition, language, motor skills, mood, and sleep (Chen et al., 2022). These findings support a case in which stimulation pulsed at 40 Hz may have unique advantages.

While forehead tPBM does not involve sensory stimulation, the use of pulsed light stimulation may directly or indirectly induce neuronal processes akin to those outlined above. Previous work using 40 Hz pulsed tPBM reported increases in EEG power across bands (Zomorrodi et al., 2019). However, to date, there has been no comparison of 10 Hz and 40 Hz in terms of their effect on alpha and gamma rhythms. While most continuous tPBM studies reported general increases in alpha and beta rhythms across frequency bands (Pruitt et al., 2024; Wang et al., 2019), we observed that 40 Hz tPBM was associated with stronger alpha-band effects and widespread beta- and gamma-band activity. These findings were not really irradiance-dependent, demonstrating the feasibility of targeting specific brain rhythms in addition to using lower power in PBM. These findings do not rule out the potential for cross-spectral coupling involving other rhythms (Shahdadian et al., 2022), although no significant pulsation-frequency dependence in other frequency bands was observed.

These results, largely driven by stimulation frequency, potentially reflect underlying frequency-specific mitochondrial responses. Tang et al. (2023) showed that 40 Hz pulsed NIR light significantly enhanced ATP production and mitochondrial membrane potential in neuron-like cells, with stronger effects than CW or other pulsed frequencies. Similarly, Kim et al. (2017) reported that 30 and 300 Hz pulsed PBM altered mitochondrial behaviour more strongly than 3 Hz, as seen by delayed intracellular responses, suggesting that mid-to-high pulse frequencies may influence mitochondrial dynamics more effectively.

4.4 The Influence of Skin Tone

Monte Carlo simulations have shown that increased melanin concentration reduces light penetration in human skin, particularly at shorter wavelengths (Cassano et al., 2019; Li et al., 2017; Palamoni et al., 2022; Van Lankveld et al., 2024). This is due to higher absorption in superficial skin layers, where melanin acts as a major absorber of visible and NIR light. Studies across different skin phenotypes and wavelengths confirm that shorter wavelengths are more sensitive to pigmentation-related attenuation (Palamoni et al., 2022; Van Lankveld et al., 2024). These findings highlight the importance of accounting for skin tone in tPBM and support the need for personalized dosimetry to optimize treatment outcomes (Palamoni et al., 2022).

Our findings strongly support the influence of skin tone in tPBM. Light skin tones (higher ITA) are consistently associated with greater EEG responses in terms of power and entropy (**Figure 12**). In fact, skin tone accounted for the largest factor by which the EEG responses varied, larger than wavelength, frequency and fluence. Moreover, we did not find a significant wavelength-ITA interaction; that is, results from the use of 808 nm wavelength were not more ITA-dependent than those based on 1064 nm wavelength. These findings establish the importance of accounting for skin tone and the potential benefits of personalizing tPBM for optimal treatment outcome. Moreover, options for light delivery that bypass skin melanin are potentially beneficial in this context. For example, while melanin is present in the nose and in the ear, the amounts are much lower than in the skin, due to the far lower numbers of melanocytes and the general lack of sun exposure (Cichorek et al., 2013).

4.5 The Influence of Wavelength

Studies have shown that different wavelengths penetrate human brain tissue to varying degrees, with 808 nm demonstrating substantial penetration (Tedford et al., 2015). As noted earlier, the interaction between wavelength and tissue response may also be influenced by skin pigmentation (Palamoni et al., 2022; Van Lankveld et al., 2024). However, beyond differences in penetration depth, the cellular response to PBM varies by wavelength, reflecting distinct biochemical effects. For instance, in dorsal root ganglion neurons, 800 nm light primarily influenced mitochondrial metabolism, whereas 970 nm light modulated nociceptive signal transmission (Zupin et al., 2019). A meta-analysis of pre-clinical studies using continuous tPBM on traumatic brain injury also found that wavelengths around 665 nm and 810 nm were most effective in improving neurological outcomes and reducing lesion size (Stevens et al., 2023), likely due to higher energy deposition in cortical tissue, as shown in Monte carlo simulations (Cassano et al., 2019), and better alignment with CCO's absorption peak (Bhattacharya and Dutta, 2019).

In our pulsed tPBM study, we found that wavelength interacted significantly with pulsation frequency. While most prior work has focused on 808 or 810 nm – believed to offer a balance between deep penetration and minimal tissue heating – our results suggest that positive EEG power changes were greatest with 1064 nm, particularly in the alpha and gamma. Further supporting the unique potential of 1064 nm stimulation, Yokomizo et al. (2022) showed that, 1064 nm PBM significantly increased NO production in human endothelial cells, in a dose-dependent manner, even at low irradiance levels (10 mW/cm^2 for 5 minutes). This was mediated through the enhancement of eNOS via mitochondrial retrograde signaling involving reactive oxygen species and Akt phosphorylation pathways. This is consistent with the trends shown by Pope et al. (2020) in retinal pigmented epithelium cells, where NO increased more for longer wavelengths in continuous-wave exposure within the NIR range. These results suggest that 1064 nm stimulation may promote neurovascular effects such as increased CBF and neuroprotection, potentially through NO-mediated vasodilation, complementing CCO-driven metabolic effects traditionally associated with tPBM. It remains unclear how NO release is related to the EEG response, which will be addressed in our future work.

4.6 Limitations and Future Work

While this study offers novel insights into how tPBM modulates EEG-based neural activity, several limitations should be addressed. Although we controlled for individual skin pigmentation, further research is needed to understand how melanin affects light delivery, especially at shorter wavelengths. Future studies should also aim to integrate tPBM-EEG findings with hemodynamic measures such as fMRI to further clarify the link between the electrophysiological and metabolic effects of tPBM. Alternative delivery routes, such as intranasal application that bypass melanin- and bone-dense tissue, also represent promising directions for enhancing NIR effectiveness. Finally, as our sample was limited to healthy young adults, it remains essential to examine how these effects generalize to older or clinical populations with altered brain dynamics.

5 CONCLUSIONS

This investigation studied the impact of key PBM parameters (wavelength, pulsation frequency, irradiance, and skin pigmentation) on EEG power and entropy in healthy young adults. We demonstrated that tPBM induces distinct frequency- and region-specific modulations in both spectral power and neural complexity, with effects influenced by both protocol design and participant characteristics. Our findings stress the importance of personalized stimulation protocols and highlight the use of EEG as a valuable tool for uncovering tPBM's neuromodulatory effects. By clarifying how these parameters interact with brain function, this work lays important groundwork for optimizing tPBM as a safe, non-invasive, and effective intervention for cognitive enhancement and neurological health.

6 ACKNOWLEDGMENTS

This work was supported by funding from the Ontario Centre for Innovation, the Natural Sciences and Engineering Research Council of Canada and Vielight Inc.

7 REFERENCES

Ai, S., Ye, S., Li, G., Leng, Y., Stone, K. L., Zhang, M., Wing, Y.-K., Zhang, J., & Liang, Y. Y. (2024). Association of disrupted delta wave activity during sleep with long-term cardiovascular disease and mortality. Journal of the American College of Cardiology, 83(17), 1671–1684. https://doi.org/10.1016/j.jacc.2024.02.040

Ando, M., Nobukawa, S., Kikuchi, M., & Takahashi, T. (2021). Identification of electroencephalogram signals in Alzheimer's disease by multifractal and multiscale entropy analysis. Frontiers in Neuroscience, 15, 667614. https://doi.org/10.3389/fnins.2021.667614

Babiloni, C., Blinowska, K., Bonanni, L., Cichocki, A., De Haan, W., Del Percio, C., Dubois, B., Escudero, J., Fernández, A., Frisoni, G., Guntekin, B., Hajos, M., Hampel, H., Ifeachor, E., Kilborn, K., Kumar, S., Johnsen, K., Johannsson, M., Jeong, J., … Randall, F. (2020). What electrophysiology tells us about Alzheimer's disease: a window into the synchronization and connectivity of brain neurons. Neurobiology of Aging, 85, 58–73. https://doi.org/10.1016/j.neurobiolaging.2019.09.008

Ballard, C., Gauthier, S., Corbett, A., Brayne, C., Aarsland, D., & Jones, E. (2011). Alzheimer's disease. Lancet, 377(9770), 1019–1031. https://doi.org/10.1016/S0140-6736(10)61349-9

Benwell, C. S. Y., Davila-Pérez, P., Fried, P. J., Jones, R. N., Travison, T. G., Santarnecchi, E., Pascual-Leone, A., & Shafi, M. M. (2020). EEG spectral power abnormalities and their relationship with cognitive dysfunction in patients with Alzheimer's disease and type 2 diabetes. Neurobiology of Aging, 85, 83–95. https://doi.org/10.1016/j.neurobiolaging.2019.10.004

Berger, H. (1929). Über das Elektrenkephalogramm des Menschen. Archiv für Psychiatrie und Nervenkrankheiten, 87(1), 527–570. https://doi.org/10.1007/bf01797193

Bhattacharya, M., & Dutta, A. (2019, July 27). Computational Modeling of the Photon Transport, Tissue Heating, and Cytochrome C Oxidase Absorption during Transcranial Near-Infrared Stimulation. https://www.mdpi.com/2076-3425/9/8/179

Brenowitz, W. D., Hubbard, R. A., Keene, C. D., Hawes, S. E., Longstreth, W. T., Jr, Woltjer, R. L., & Kukull, W. A. (2017). Mixed neuropathologies and estimated rates of clinical progression in a large autopsy sample. Alzheimer's & Dementia: The Journal of the Alzheimer's Association, 13(6), 654–662. https://doi.org/10.1016/j.jalz.2016.09.015

Buschman, T. J., & Miller, E. K. (2007). Top-down versus bottom-up control of attention in the prefrontal and posterior parietal cortices. Science (New York, N.Y.), 315(5820), 1860–1862. https://doi.org/10.1126/science.1138071

Cacciotti, A., Pappalettera, C., Miraglia, F., Rossini, P. M., & Vecchio, F. (2024). EEG entropy insights in the context of physiological aging and Alzheimer's and Parkinson's diseases: a comprehensive review. GeroScience, 46(6), 5537–5557. https://doi.org/10.1007/s11357-024-01185-1

Cao, J., Zhu, B., Zheng, K., He, S., Meng, L., Song, J., & Yang, H. (2019). Recent progress in NIR-II contrast agent for biological imaging. Frontiers in Bioengineering and Biotechnology, 7, 487. https://doi.org/10.3389/fbioe.2019.00487

Cassano, P., Tran, A. P., Katnani, H., Bleier, B. S., Hamblin, M. R., Yuan, Y., & Fang, Q. (2019). Selective photobiomodulation for emotion regulation: model-based dosimetry study. Neurophotonics, 6(1), 015004. https://doi.org/10.1117/1.NPh.6.1.015004

Chan, A. S., Lee, T. L., Yeung, M. K., & Hamblin, M. R. (2019). Photobiomodulation improves the frontal cognitive function of older adults. International Journal of Geriatric Psychiatry, 34(2), 369–377. https://doi.org/10.1002/gps.5039

Chan, D., Suk, H.-J., Jackson, B. L., Milman, N. P., Stark, D., Klerman, E. B., Kitchener, E., Fernandez Avalos, V. S., de Weck, G., Banerjee, A., Beach, S. D., Blanchard, J., Stearns, C., Boes, A. D., Uitermarkt, B., Gander, P., Howard, M., 3rd, Sternberg, E. J., Nieto-Castanon, A., … Tsai, L.-H. (2022). Gamma frequency sensory stimulation in mild probable Alzheimer's dementia patients: Results of feasibility and pilot studies. PloS One, 17(12), e0278412. https://doi.org/10.1371/journal.pone.0278412

Chen, X., Shi, X., Wu, Y., Zhou, Z., Chen, S., Han, Y., & Shan, C. (2022). Gamma oscillations and application of 40-Hz audiovisual stimulation to improve brain function. Brain and Behavior, 12(12), e2811. https://doi.org/10.1002/brb3.2811

Cheng, Q., Yang, W., Liu, K., Zhao, W., Wu, L., Lei, L., Dong, T., Hou, N., Yang, F., Qu, Y., & Yang, Y. (2019, July 16). Increased Sample Entropy in EEGs During the Functional Rehabilitation of an Injured Brain. https://www.mdpi.com/1099-4300/21/7/698

Chinnathambi, S., & Shirahata, N. (2019). Recent advances on fluorescent biomarkers of near-infrared quantum dots for in vitro and in vivo imaging. Science and Technology of Advanced Materials, 20(1), 337–355. https://doi.org/10.1080/14686996.2019.1590731

Cichorek, M., Wachulska, M., Stasiewicz, A., & Tymińska, A. (2013). Skin melanocytes: biology and development. Postepy Dermatologii i Alergologii, 30(1), 30–41. https://doi.org/10.5114/pdia.2013.33376

Delorme, A., & Makeig, S. (2004). EEGLAB: an open source toolbox for analysis of single-trial EEG dynamics including independent component analysis. Journal of Neuroscience Methods, 134(1), 9–21. https://doi.org/10.1016/j.jneumeth.2003.10.009

Dmochowski, G. M., Shereen, A. D., Berisha, D., & Dmochowski, J. P. (2020). Near-infrared light increases functional connectivity with a non-thermal mechanism. Cerebral Cortex Communications, 1(1), tgaa004. https://doi.org/10.1093/texcom/tgaa004

Engel, A. K., & Fries, P. (2010). Beta-band oscillations--signalling the status quo? Current Opinion in Neurobiology, 20(2), 156–165. https://doi.org/10.1016/j.conb.2010.02.015

Fekri, A., Jahan, A., Moghadam Salimi, M., & Oskouei, A. E. (2019). Short-term effects of transcranial near-infrared photobiomodulation on motor performance in healthy human subjects: An experimental SingleBlind randomized clinical trial. Journal of Lasers in Medical Sciences, 10(4), 317–323. https://doi.org/10.15171/jlms.2019.51

Finnigan, S., & Robertson, I. H. (2011). Resting EEG theta power correlates with cognitive performance in healthy older adults. Psychophysiology, 48(8), 1083–1087. https://doi.org/10.1111/j.1469-8986.2010.01173.x

Gal, S., Coldham, Y., Tik, N., Bernstein-Eliav, M., & Tavor, I. (2022). Act natural: Functional connectivity from naturalistic stimuli fMRI outperforms resting-state in predicting brain activity. NeuroImage, 258(119359), 119359. https://doi.org/10.1016/j.neuroimage.2022.119359

Garcia-Rill, E., D'Onofrio, S., Luster, B., Mahaffey, S., Urbano, F. J., & Phillips, C. (2016). The 10 Hz frequency: A fulcrum for transitional brain states. Translational Brain Rhythmicity, 1(1), 7–13. https://doi.org/10.15761/tbr.1000103

Gasser, T., Verleger, R., Bächer, P., & Sroka, L. (1988). Development of the EEG of school-age children and adolescents. I. Analysis of band power. Electroencephalography and Clinical Neurophysiology, 69(2), 91–99. https://doi.org/10.1016/0013-4694(88)90204-0

Ghaderi, A. H., Jahan, A., Akrami, F., & Moghadam Salimi, M. (2021). Transcranial photobiomodulation changes topology, synchronizability, and complexity of resting state brain networks. Journal of Neural Engineering, 18(4), 046048. https://doi.org/10.1088/1741-2552/abf97c

Gillespie, J. B., Maclean, M., Given, M. J., Wilson, M. P., Judd, M. D., Timoshkin, I. V., & MacGregor, S. J. (2017). Efficacy of pulsed 405-nm light-emitting diodes for antimicrobial photodynamic inactivation: Effects of intensity, frequency, and duty cycle. Photomedicine and Laser Surgery, 35(3), 150–156. https://doi.org/10.1089/pho.2016.4179

Gonzalez-Lima, F., & Barrett, D. W. (2014). Augmentation of cognitive brain functions with transcranial lasers. Frontiers in Systems Neuroscience, 8, 36. https://doi.org/10.3389/fnsys.2014.00036

Grin-Yatsenko, V. A., Baas, I., Ponomarev, V. A., & Kropotov, J. D. (2009). EEG power spectra at early stages of depressive disorders. Journal of Clinical Neurophysiology: Official Publication of the American Electroencephalographic Society, 26(6), 401–406. https://doi.org/10.1097/WNP.0b013e3181c298fe

Hainke, L., Dowsett, J., Spitschan, M., & Priller, J. (2025). 40 Hz visual stimulation during sleep evokes neuronal gamma activity in NREM and REM stages. Sleep, 48(3). https://doi.org/10.1093/sleep/zsae299

Hall, J. D., Green, J. M., Chen, Y.-C. A., Liu, Y., Zhang, H., Sundman, M. H., & Chou, Y.-H. (2024). Exploring the potential of combining transcranial magnetic stimulation and electroencephalography to investigate mild cognitive impairment and Alzheimer's disease: a systematic review. GeroScience, 46(4), 3659–3693. https://doi.org/10.1007/s11357-024-01075-6

Hamblin, M. R. (2016). Shining light on the head: Photobiomodulation for brain disorders. BBA Clinical, 6, 113–124. https://doi.org/10.1016/j.bbacli.2016.09.002

Hamblin, M. R. (2018). Mechanisms and mitochondrial redox signaling in photobiomodulation. Photochemistry and Photobiology, 94(2), 199–212. https://doi.org/10.1111/php.12864

Hashmi, J. T., Huang, Y.-Y., Sharma, S. K., Kurup, D. B., De Taboada, L., Carroll, J. D., & Hamblin, M. R. (2010). Effect of pulsing in low-level light therapy. Lasers in Surgery and Medicine, 42(6), 450–466. https://doi.org/10.1002/lsm.20950

Helfrich, R. F., Schneider, T. R., Rach, S., Trautmann-Lengsfeld, S. A., Engel, A. K., & Herrmann, C. S. (2014). Entrainment of brain oscillations by transcranial alternating current stimulation. Current Biology: CB, 24(3), 333–339. https://doi.org/10.1016/j.cub.2013.12.041

Henderson, T. A., & Morries, L. D. (2015). Near-infrared photonic energy penetration: can infrared phototherapy effectively reach the human brain? Neuropsychiatric Disease and Treatment, 11, 2191–2208. https://doi.org/10.2147/NDT.S78182

Hennessy, M., & Hamblin, M. R. (2017). Photobiomodulation and the brain: a new paradigm. Journal of Optics (2010), 19(1), 013003. https://doi.org/10.1088/2040-8986/19/1/013003

Hess, C., Levy, B., Hashmi, A. Z., Hogan, J., Greenspan, S., Elber, A., Falcon, K., & Driscoll, D. F. (2020). Subjective versus objective assessment of cognitive functioning in primary care. Journal of the American Board of Family Medicine: JABFM, 33(3), 417–425. https://doi.org/10.3122/jabfm.2020.03.190265

Hopfinger, J. B. (2017). Relation of higher-frequency oscillatory activity to white matter changes and to core mechanisms of attention. Cognitive Neuroscience, 8(2), 124–126. https://doi.org/10.1080/17588928.2016.1195803

Huang, Y.-Y., Chen, A. C.-H., Carroll, J. D., & Hamblin, M. R. (2009). Biphasic dose response in low level light therapy. Dose-Response: A Publication of International Hormesis Society, 7(4), 358–383. https://doi.org/10.2203/dose-response.09-027.Hamblin

Iaccarino, H. F., Singer, A. C., Martorell, A. J., Rudenko, A., Gao, F., Gillingham, T. Z., Mathys, H., Seo, J., Kritskiy, O., Abdurrob, F., Adaikkan, C., Canter, R. G., Rueda, R., Brown, E. N., Boyden, E. S., & Tsai, L.-H. (2016). Gamma frequency entrainment attenuates amyloid load and modifies microglia. Nature, 540(7632), 230–235. https://doi.org/10.1038/nature20587

Jabès, A., Klencklen, G., Ruggeri, P., Antonietti, J.-P., Banta Lavenex, P., & Lavenex, P. (2021). Age-related differences in resting-state EEG and allocentric spatial working memory performance. Frontiers in Aging Neuroscience, 13, 704362. https://doi.org/10.3389/fnagi.2021.704362

Jackson, C. E., & Snyder, P. J. (2008). Electroencephalography and event-related potentials as biomarkers of mild cognitive impairment and mild Alzheimer's disease. Alzheimer's & Dementia: The Journal of the Alzheimer's Association, 4(1 Suppl 1), S137-43. https://doi.org/10.1016/j.jalz.2007.10.008

Jahan, A., Nazari, M. A., Mahmoudi, J., Salehpour, F., & Salimi, M. M. (2019). Transcranial near-infrared photobiomodulation could modulate brain electrophysiological features and attentional performance in healthy young adults. Lasers in Medical Science, 34(6), 1193–1200. https://doi.org/10.1007/s10103-018-02710-3

Jeong, J. (2004). EEG dynamics in patients with Alzheimer's disease. Clinical Neurophysiology: Official Journal of the International Federation of Clinical Neurophysiology, 115(7), 1490–1505. https://doi.org/10.1016/j.clinph.2004.01.001

Jung, G., Kim, S., Lee, J., & Yoo, S. (2023). Generation of skin tone and pigmented region-modified images using a pigment discrimination model trained with an optical approach. Skin Research and Technology, 29(10), e13486. https://doi.org/10.1111/srt.13486

Kashiwagi, S., Brauns, T., Gelfand, J., & Poznansky, M. C. (2014). Laser vaccine adjuvants. History, progress, and potential. Human Vaccines & Immunotherapeutics, 10(7), 1892–1907. https://doi.org/10.4161/hv.28840

Kim, H. B., Baik, K. Y., Choung, P.-H., & Chung, J. H. (2017). Pulse frequency dependency of photobiomodulation on the bioenergetic functions of human dental pulp stem cells. Scientific Reports, 7(1), 15927. https://doi.org/10.1038/s41598-017-15754-2

Klimesch, W., Doppelmayr, M., Pachinger, T., & Ripper, B. (1997). Brain oscillations and human memory: EEG correlates in the upper alpha and theta band. Neuroscience Letters, 238(1–2), 9–12. https://doi.org/10.1016/s0304-3940(97)00771-4

Knyazev, G. G. (2012). EEG delta oscillations as a correlate of basic homeostatic and motivational processes. Neuroscience and Biobehavioral Reviews, 36(1), 677–695. https://doi.org/10.1016/j.neubiorev.2011.10.002

Li, T., Xue, C., Wang, P., Li, Y., & Wu, L. (2017). Photon penetration depth in human brain for light stimulation and treatment: A realistic Monte Carlo simulation study. Journal of Innovative Optical Health Sciences, 10(05), 1743002. https://doi.org/10.1142/s1793545817430027

Liu, C., Han, T., Xu, Z., Liu, J., Zhang, M., Du, J., Zhou, Q., Duan, Y., Li, Y., Wang, J., Cui, D., & Wang, Y. (2022). Modulating gamma oscillations promotes brain connectivity to improve cognitive impairment. Cerebral Cortex (New York, N.Y.: 1991), 32(12), 2644–2656. https://doi.org/10.1093/cercor/bhab371

López-Loeza, E., Rangel-Argueta, A. R., López-Vázquez, M. Á., Cervantes, M., & Olvera-Cortés, M. E. (2016). Differences in EEG power in young and mature healthy adults during an incidental/spatial learning task are related to age and execution efficiency. Age (Dordrecht, Netherlands), 38(2), 37. https://doi.org/10.1007/s11357-016-9896-z

Mahjoory, K., Cesnaite, E., Hohlefeld, F. U., Villringer, A., & Nikulin, V. V. (2019). Power and temporal dynamics of alpha oscillations at rest differentiate cognitive performance involving sustained and phasic cognitive control. NeuroImage, 188, 135–144. https://doi.org/10.1016/j.neuroimage.2018.12.001

McDonough, I. M., & Nashiro, K. (2014). Network complexity as a measure of information processing across resting-state networks: evidence from the Human Connectome Project. Frontiers in Human Neuroscience, 8, 409. https://doi.org/10.3389/fnhum.2014.00409

Mizuno, T., Takahashi, T., Cho, R. Y., Kikuchi, M., Murata, T., Takahashi, K., & Wada, Y. (2010). Assessment of EEG dynamical complexity in Alzheimer's disease using multiscale entropy. Clinical Neurophysiology: Official Journal of the International Federation of Clinical Neurophysiology, 121(9), 1438–1446. https://doi.org/10.1016/j.clinph.2010.03.025

Nunez, P. L., & Srinivasan, R. (2005). Electric fields of the brain (2nd ed.). Oxford University Press. https://doi.org/10.1093/acprof:oso/9780195050387.001.0001

Oostenveld, R., Fries, P., Maris, E., & Schoffelen, J.-M. (2011). FieldTrip: Open source software for advanced analysis of MEG, EEG, and invasive electrophysiological data. Computational Intelligence and Neuroscience, 2011, 156869. https://doi.org/10.1155/2011/156869

Palamoni, O. P., de Magalhães, A. C., Moriyama, L. T., Sousa, M. V. P. de, & Fortunato, T. C. (2022). Monte Carlo simulations to study light propagation through the skin of different phototypes. In Z. Zalevsky, V. V. Tuchin, & W. C. Blondel (Eds.), Tissue Optics and Photonics II. SPIE. https://doi.org/10.1117/12.2621670

Palva, J. M., Monto, S., Kulashekhar, S., & Palva, S. (2010). Neuronal synchrony reveals working memory networks and predicts individual memory capacity. Proceedings of the National Academy of Sciences of the United States of America, 107(16), 7580–7585. https://doi.org/10.1073/pnas.0913113107

Park, J. M., & Tsai, L.-H. (2025). Innovations in noninvasive sensory stimulation treatments to combat Alzheimer's disease. PLoS Biology, 23(2), e3003046. https://doi.org/10.1371/journal.pbio.3003046

Pogue, B. W., Lilge, L., Patterson, M. S., Wilson, B. C., & Hasan, T. (1997). Absorbed photodynamic dose from pulsed versus continuous wave light examined with tissue-simulating dosimeters. Applied Optics, 36(28), 7257–7269. https://doi.org/10.1364/ao.36.007257

Pope, N. J., Powell, S. M., Wigle, J. C., & Denton, M. L. (2020). Wavelength- and irradiance-dependent changes in intracellular nitric oxide level. Journal of Biomedical Optics, 25(8), 1–20. https://doi.org/10.1117/1.JBO.25.8.085001

Pruitt, T., Davenport, E. M., Proskovec, A. L., Maldjian, J. A., & Liu, H. (2024). Simultaneous MEG and EEG source imaging of electrophysiological activity in response to acute transcranial photobiomodulation. Frontiers in Neuroscience, 18, 1368172. https://doi.org/10.3389/fnins.2024.1368172

Pruitt, T., Wang, X., Wu, A., Kallioniemi, E., Husain, M. M., & Liu, H. (2020). Transcranial photobiomodulation (tPBM) with 1,064-nm laser to improve cerebral metabolism of the human brain in vivo. Lasers in Surgery and Medicine, 52(9), 807–813. https://doi.org/10.1002/lsm.23232

R.E. Dustman, D.E. Shearer, Y. Emmerson. (n.d.). EEG and event-related potentials in normal aging. Retrieved May 20, 2025, from https://www.sciencedirect.com/science/article/pii/030100829390005D?via=ihub

Richman, J. S., & Moorman, J. R. (2000). Physiological time-series analysis using approximate entropy and sample entropy. American Journal of Physiology. Heart and Circulatory Physiology, 278(6), H2039-49. https://doi.org/10.1152/ajpheart.2000.278.6.H2039

Salehpour, F., Mahmoudi, J., Kamari, F., Sadigh-Eteghad, S., Rasta, S. H., & Hamblin, M. R. (2018). Brain photobiomodulation therapy: A narrative review. Molecular Neurobiology, 55(8), 6601–6636. https://doi.org/10.1007/s12035-017-0852-4

Sandell, J. L., & Zhu, T. C. (2011). A review of in-vivo optical properties of human tissues and its impact on PDT. Journal of Biophotonics, 4(11–12), 773–787. https://doi.org/10.1002/jbio.201100062

Sargent, K., Chavez-Baldini, U., Master, S. L., Verweij, K. J. H., Lok, A., Sutterland, A. L., Vulink, N. C., Denys, D., Smit, D. J. A., & Nieman, D. H. (2021). Resting-state brain oscillations predict cognitive function in psychiatric disorders: A transdiagnostic machine learning approach. NeuroImage. Clinical, 30(102617), 102617. https://doi.org/10.1016/j.nicl.2021.102617

Scally, B., Burke, M. R., Bunce, D., & Delvenne, J.-F. (2018). Resting-state EEG power and connectivity are associated with alpha peak frequency slowing in healthy aging. Neurobiology of Aging, 71, 149–155. https://doi.org/10.1016/j.neurobiolaging.2018.07.004

Scott, J. A., Kalra, A., Pratiher, D., Berman, M., & Wood, S. (2024). Design and validation of EEG biomarkers for transcranial photobiomodulation. In J. D. Carroll, A. Liebert, & J.-A. Lyons (Eds.), Mechanisms of Photobiomodulation Therapy XVIII. SPIE. https://doi.org/10.1117/12.3021832

Shahdadian, S., Wang, X., Wanniarachchi, H., Chaudhari, A., Truong, N. C. D., & Liu, H. (2022). Neuromodulation of brain power topography and network topology by prefrontal transcranial photobiomodulation. Journal of Neural Engineering, 19(6), 066013. https://doi.org/10.1088/1741-2552/ac9ede

Shetty, S. J., Shetty, S., Shettigar, D., Pagilla, V., & Maiya, G. A. (2023). Effect of transcranial photobiomodulation on electrophysiological activity of brain in healthy individuals: A scoping review. Journal of Clinical Neuroscience: Official Journal of the Neurosurgical Society of Australasia, 117, 156–167. https://doi.org/10.1016/j.jocn.2023.09.029

Smit, D. J. A., Posthuma, D., Boomsma, D. I., & De Geus, E. J. C. (2009). Phenotypic and genetic correlations between evoked EEG/ERP measures during the response anticipation period of a delayed response task. Psychophysiology, 46(2), 344–356. https://doi.org/10.1111/j.1469-8986.2008.00777.x

Spera, V., Sitnikova, T., Ward, M. J., Farzam, P., Hughes, J., Gazecki, S., Bui, E., Maiello, M., De Taboada, L., Hamblin, M. R., Franceschini, M. A., & Cassano, P. (2021). Pilot study on dose-dependent effects of transcranial photobiomodulation on brain electrical oscillations: A potential therapeutic target in Alzheimer's disease. Journal of Alzheimer's Disease: JAD, 83(4), 1481–1498. https://doi.org/10.3233/JAD-210058

Stacey, J. E., Crook-Rumsey, M., Sumich, A., Howard, C. J., Crawford, T., Livne, K., Lenzoni, S., & Badham, S. (2021). Age differences in resting state EEG and their relation to eye movements and cognitive performance. Neuropsychologia, 157(107887), 107887. https://doi.org/10.1016/j.neuropsychologia.2021.107887

Stevens, A. R., Hadis, M., Milward, M., Ahmed, Z., Belli, A., Palin, W., & Davies, D. J. (2023). Photobiomodulation in acute traumatic brain injury: A systematic review and meta-analysis. Journal of Neurotrauma, 40(3–4), 210–227. https://doi.org/10.1089/neu.2022.0140

Tang, L., Jiang, H., Sun, M., & Liu, M. (2023). Pulsed transcranial photobiomodulation generates distinct beneficial neurocognitive effects compared with continuous wave transcranial light. Lasers in Medical Science, 38(1), 203. https://doi.org/10.1007/s10103-023-03865-4

Tedford, C. E., DeLapp, S., Jacques, S., & Anders, J. (2015). Quantitative analysis of transcranial and intraparenchymal light penetration in human cadaver brain tissue. Lasers in Surgery and Medicine, 47(4), 312–322. https://doi.org/10.1002/lsm.22343

Van Lankveld, H., Mai, A. Q., Lim, L., Hosseinkhah, N., Cassano, P., & Jean Chen, J. (2024). Simulation-based dosimetry of transcranial and intranasal photobiomodulation of the human brain: the roles of wavelength, power density and skin colour. In bioRxiv. https://doi.org/10.1101/2024.04.05.588330

Vargas, E., Barrett, D. W., Saucedo, C. L., Huang, L.-D., Abraham, J. A., Tanaka, H., Haley, A. P., & Gonzalez-Lima, F. (2017). Beneficial neurocognitive effects of transcranial laser in older adults. Lasers in Medical Science, 32(5), 1153–1162. https://doi.org/10.1007/s10103-017-2221-y

Vlahou, E. L., Thurm, F., Kolassa, I.-T., & Schlee, W. (2014). Resting-state slow wave power, healthy aging and cognitive performance. Scientific Reports, 4(1), 5101. https://doi.org/10.1038/srep05101

Wach, C., Krause, V., Moliadze, V., Paulus, W., Schnitzler, A., & Pollok, B. (2013). Effects of 10 Hz and 20 Hz transcranial alternating current stimulation (tACS) on motor functions and motor cortical excitability. Behavioural Brain Research, 241, 1–6. https://doi.org/10.1016/j.bbr.2012.11.038

Wang, X., Dmochowski, J. P., Zeng, L., Kallioniemi, E., Husain, M., Gonzalez-Lima, F., & Liu, H. (2019). Transcranial photobiomodulation with 1064-nm laser modulates brain electroencephalogram rhythms. Neurophotonics, 6(2), 025013. https://doi.org/10.1117/1.NPh.6.2.025013

Wang, X., Tian, F., Soni, S. S., Gonzalez-Lima, F., & Liu, H. (2016). Interplay between up-regulation of cytochrome-c-oxidase and hemoglobin oxygenation induced by near-infrared laser. Scientific Reports, 6(1). https://doi.org/10.1038/srep30540

Yang, A. C., Jann, K., Michel, C. M., & Wang, D. J. J. (2020). Editorial: Advances in multi-scale analysis of brain complexity. Frontiers in Neuroscience, 14, 337. https://doi.org/10.3389/fnins.2020.00337

Yokomizo, S., Roessing, M., Morita, A., Kopp, T., Ogawa, E., Katagiri, W., Feil, S., Huang, P. L., Atochin, D. N., & Kashiwagi, S. (2022). Near-infrared II photobiomodulation augments nitric oxide bioavailability via phosphorylation of endothelial nitric oxide synthase. FASEB Journal: Official Publication of the Federation of American Societies for Experimental Biology, 36(9), e22490. https://doi.org/10.1096/fj.202101890R

Zein, R., Selting, W., & Hamblin, M. R. (2018). Review of light parameters and photobiomodulation efficacy: dive into complexity. Journal of Biomedical Optics, 23(12), 1. https://doi.org/10.1117/1.jbo.23.12.120901

Zhang, H., Geng, X., Wang, Y., Guo, Y., Gao, Y., Zhang, S., Du, W., Liu, L., Sun, M., Jiao, F., Yi, F., Li, X., & Wang, L. (2021). The significance of EEG alpha oscillation spectral power and beta oscillation phase synchronization for diagnosing probable Alzheimer disease. Frontiers in Aging Neuroscience, 13, 631587. https://doi.org/10.3389/fnagi.2021.631587

Zheng, H., Onoda, K., Nagai, A., & Yamaguchi, S. (2020). Reduced dynamic complexity of BOLD signals differentiates mild cognitive impairment from normal aging. Frontiers in Aging Neuroscience, 12, 90. https://doi.org/10.3389/fnagi.2020.00090

Zomorrodi, R., Loheswaran, G., Pushparaj, A., & Lim, L. (2019). Pulsed Near Infrared Transcranial and Intranasal Photobiomodulation Significantly Modulates Neural Oscillations: a pilot exploratory study. Scientific Reports, 9(1), 6309. https://doi.org/10.1038/s41598-019-42693-x

Zúñiga, M. A., Acero-González, Á., Restrepo-Castro, J. C., Uribe-Laverde, M. Á., Botero-Rosas, D. A., Ferreras, B. I., Molina-Borda, M. C., & Villa-Reyes, M. P. (2024). Is EEG entropy a useful measure for Alzheimer's disease? Actas Espanolas de Psiquiatria, 52(3), 347–364. https://doi.org/10.62641/aep.v52i3.1632

Zupin, L., Ottaviani, G., Rupel, K., Biasotto, M., Zacchigna, S., Crovella, S., & Celsi, F. (2019). Analgesic effect of Photobiomodulation Therapy: An in vitro and in vivo study. Journal of Biophotonics, 12(10), e201900043. https://doi.org/10.1002/jbio.201900043